REPETITION-RATE STABILIZATION OF A FEMTOSECOND STRETCHED-SPECTRUM FIBER LASER

A THESIS SUBMITTED TO

THE DEPARTMENT OF PHYSICS

AND THE INSTITUTE OF ENGINEERING AND SCIENCE

OF BILKENT UNIVERSITY

IN PARTIAL FULFILLMENT OF THE REQUIREMENTS

FOR THE DEGREE OF

MASTER OF SCIENCE

By

Coşkun Ülgüdür

August, 2008

I certify that I have read this thesis and that in my opinion it is fully adequate, in scope and in quality, as a thesis for the degree of master of science.

Asst. Prof. Dr. Fatih Ömer İlday

I certify that I have read this thesis and that in my opinion it is fully adequate, in scope and in quality, as a thesis for the degree of master of science.

Asst. Prof. Dr. Mehmet Özgür Oktel

I certify that I have read this thesis and that in my opinion it is fully adequate, in scope and in quality, as a thesis for the degree of master of science.

Instructor Hakan Altan

Approved for the Institute of Engineering and Science:

_____

Prof. Dr. Mehmet B. Baray

Director of the Institute

ABSTRACT

REPETITION-RATE STABILIZATION OF A FEMTOSECOND STRETCHED-SPECTRUM FIBER LASER

Coşkun Ülgüdür

M.S. in Physics

Supervisor: Asst. Prof. Dr. Fatih Ömer İlday

August, 2008

Passively modelocked lasers produce trains of femtosecond pulses, with the temporal separation between the pulses being determined by the length of the laser cavity. The repetition rate of the laser is inverse of this temporal separation. For a free-running laser, the repetition rate is very stable over short time scales (less than 1 ms), but drifts due to environmental effects on a longer time scale. For applications demanding a precise repetition rate to be maintained, such as optical frequency metrology, the laser needs to be locked to an RF or microwave reference source with a feedback loop acting on an actuator within the laser cavity.

In this work, repetition-rate stabilization of a "stretched-spectrum" fiber laser is reported, which corresponds to a new modelocking regime. As the name implies, the laser produces pulses undergoing periodic breathing of the spectra during a complete round trip through the cavity. To the best of our knowledge, this breathing is the strongest modification observed in a laser to date. It is noteworthy that even under such strong nonlinearity the laser is more robust than the regular stretched-pulse laser.

Encouraged with its robustness, it is proposed that the stretched-spectrum fiber laser is a promising alternate to laser oscillators for frequency metrology applications and laser master oscillators in use with accelerator based next-generation light sources. After photodetection of the laser output, one of the upper harmonics of the laser is locked to a highly stable dielectric resonator oscillator (DRO) at 1.3 GHz. In order to reduce the environmental effects on the laser, a handmade encasing was developed and temperature control of the fibers in the cavity was implemented. Remarkably, the custom encasing of the laser dramatically improved the laser's stability, outperforming the DRO up to a 5 kHz bandwidth. Since the heating-loop is not sensitive enough, latter upgrade does not decrease the phase noise of the laser, but ensures the temperature stability stays within limits in unclimatized environment. With the present setup, we observe a maximum locking range of a few kHz. The system has the potential to stay in-lock indefinitely, as long as the excessive perturbations on the system are prevented.

Keywords: Femtosecond fiber laser, stretched-spectrum fiber laser, laser phase noise, laser repetition rate, repetition-rate locking, phase-locked loop

ÖZET

FEMTOSANİYE, GERİLMİŞ TAYFLI FİBER LAZERDE TEKRAR FREKANSININ DENGELENMESİ

Coşkun Ülgüdür

Fizik Yüksek Lisans

Tez Yöneticisi: Asst. Prof. Dr. Fatih Ömer İlday

Ağustos, 2008

Pasif olarak mod kilitli lazerler femtosaniye atım dizisi oluşturur. Bu atımların zamansal aralıklarını lazer kovuğunun uzunluğu belirler. Lazerin tekrar frekansı bu zamansal aralığın tersidir. Serbest hareketli lazerlerde, tekrar frekansı kısa zaman dilimlerinde (1ms'den daha az) oldukça kararlı olmasına rağmen çevresel faktörlerden dolayı daha büyük zaman dilimlerinde sapar. Optik frekans ölçme bilimi gibi tekrar frekansının kesin olarak belirli olması gereken uygulamalar için lazer bir geribesleme döngüsü ile RF ya da mikrodalga referans kaynağa kilitlenir.

Bu çalışmada yeni bir mod kilitleme rejimi olan gerilmiş tayflı bir fiber lazerin tekrar frekansının dengelenmesi bildiriliyor. İsmi işaret ettiği gibi, bu lazer kovuk içinde bir tur boyunca periyodik olarak daralıp genişleyen tayfa sahip atımlar üretir. Bilgimiz dahilinde bu daralıp genişleme şimdiye kadar bir lazer de gözlemlenmiş en güçlü değişimdir. Bu derece yüksek doğrusal olmayan etkilerde bile lazerin normal bir gerilmiş atımlı lazere nazaran daha sağlam olması dikkate değer.

Sağlamlığından cesaret alarak, gerilmiş tayflı fiber lazerin frekans ölçüm bilimi ve hızlandırıcı tabanlı yeni nesil ışık kaynağı uygulamalarında umut veren alternatif lazer

salıngaç olduğu öneriliyor. Lazer çıktısının fotoseziminden sonra üst harmoniklerinden biri 1.3 GHz'de çalışan, yüksek derecede kararlı bir dielektrik çınlaç salıngacına (DRO) kilitlenir. Lazer üzerindeki çevresel faktörleri azaltmak için, el yapımı bir kutulama yapılmış ve kovuk içindeki fiberlerin sıcaklık kontrolü sağlanmıştır. Lazerin kutulanması kararlılığını dramatik olarak arttırmış, 5kHz bant aralığına kadar DRO'dan daha kararlı olmuştur. Sıcaklık kontrolü yeteri kadar hassas olmadığından, lazer faz gürültüsünü azaltmamış, fakat klimasız ortamda lazer sıcaklığının limitler içinde kalmasını sağlamıştır. Şu anki kurulumla, en fazla birkaç kHz kilitleme sınırı elde edilmektedir. Aşırı rahatsızlıklar engellenirse sistem potensiyel olarak sonsuza kadar kilitli kalabilir.

Anahtar sözcükler: Femtosaniye fiber lazer, gerilmiş tayflı fiber lazer, lazer faz gürültüsü, lazer tekrar frekansı, tekrar frekansı kilitleme, faz kilitli döngü

Acknowledgement

Firstly I would like to thank my academic advisor Fatih Ömer İlday for his enthusiastic support of my thesis. His assistance at various points of the thesis carved the way it is finalized. Apart for his invaluable support, I would also like to thank him for the excellence of the working environment he provided in less than a year. The Ultrafast Lasers Group of Bilkent University would not be one of the pinnacles in its subject without his efforts to improve its facilities.

I am indebted to the members of the Ultrafast Lasers Group, Pranab Mukhopadhyay, Bastian Lorbeer, Alper Bayrı, İ. Levent Budunoğlu, Bülent Öktem, Kıvanç Özgören, Seydi Yavaş and Çağrı Şenel for providing a high standard scientific environment and for supporting me at various points of the thesis.

I want to express my special thanks to İ. Levent Budunoğlu for his friendship and support through the long days and nights of work. Thanks to our collaboration in laser noise measurements, most enlightening ideas come up during our discussions.

I am particularly grateful to Bülent Öktem for his support in numerical simulations part of the thesis. The initial parameters I used for my system were originally from his previous studies which helped me a great deal.

I wish to express my special thanks to Alper Bayri for his friendship and engineering support throughout the thesis. I am indebted to him for assisting me in the temperature control setup of the laser. His fast response in my orders of new equipment saved me days of invaluable time.

I am particularly grateful to Bastian Lorbeer for his support in electronics and technical discussions we had constantly for improving my setup.

I would like to thank Kıvanç Özgören for his friendship and for sharing his experience at various problems I encountered in the thesis.

Many thanks go to Dr. Aykutlu Dana for lending me his group's power amplifier and for helping me about the problems I had with it.

I would also like to thank Paolo Sigalotti @FERMI Laser Group and Dr. Axel Winter @DESY for their introduction to phase-locked loops and noise phenomena in lasers. Their initial guidance helped me a lot throughout my studies.

I am grateful to Çağrı Şenel for his efforts on optimizing the numerical simulation algorithm for our needs and for writing the GUI of the simulation to let us use it efficiently.

Last but not the least I would like to thank all the members of Ultrafast Lasers Group for their lenience in my frequent use of public measurement devices and optic components toward the end of my thesis studies.

Finally, I wish to thank and acknowledge my thesis examination committee: Asst. Prof. Dr. Fatih Ömer İlday, Asst. Prof. Dr. Mehmet Özgür Oktel and Asst. Prof. Dr. Hakan Altan.

This work was supported by the Bilkent University, Department of Physics, Ultrafast Lasers Group and Turkish Scientific and Technical Research Council (TÜBİTAK).

Contents

CONTENTS

List of Figures

LIST OF FIGURES

Chapter 1

Introduction

1.1. Brief History of Fiber Lasers

19^{th} century hosts the origins of telecommunications. First the demonstration of telegraph by Samuel Morse in 1837, following the first telephone exchange operated by Alexander Graham Bell in 1878 initiated the rapid discoveries of communication means. James C. Maxwell's clarification of "Maxwell's Equations" in 1878 led to the discovery of radio waves by Heinrich Hertz in 1888 and in 1895 the first radio is demonstrated by Guglielmo Marconi. Early radio has a bandwidth 15 kHz and after more than a century the maximum bandwidth of wireless communication is still around a few hundred MHz. The reason is that free space propagation of signals is not suitable for reliable/fast communication links. The solution to this problem is to use a waveguide for light (information) propagation hence avoiding distortions present in free space. The basic phenomenon responsible for guiding of light in waveguides is total internal reflection. Optical fibers, the most common waveguides, were first fabricated uncladded in 1920s. However the real origin of fiber optics was not born until the first usage of cladding layer on optical fibers in 1950s. The use of cladding substantially improved the fiber performance. Nevertheless it is the use of low-loss silica in fiber fabrication that lets losses around 0.2 dB/km in the telecommunication wavelength, 1.5 μm.

The developments in optical fibers led not only to advancements in telecommunications, but also to the birth of a new field, nonlinear fiber optics. Studies of nonlinear phenomena in optical fibers such as Stimulated Raman- and Brillouin-scattering, optically induced birefringence, parametric four-wave mixing and self-phase modulation were conducted in 1970s [1-7]. An important milestone was that in 1973, it was suggested that optical fibers can support soliton-like pulses by the interplay between nonlinear and dispersive effects of fibers [8]. Optical solitons were first observed in a 1980 experiment [9] and led to further advances in the field of nonlinear optics. The field continued to grow in 1990s, especially after the fabrication of optical fibers doped with rare-earth elements (Erbium, ytterbium, etc). Fiber laser oscillators were the next phase in the field of nonlinear optics. However one problem was that soliton-like mode-locking regime in fiber lasers has severe limitations in terms of pulse energy and duration [10, 11]. Several other mode-locking regimes (dispersion-managed/stretched-pulse [12], similariton [13, 14], all-normal GVD [15]) have been demonstrated in recent years, which overcome many of these limitations. Using these new approaches, optimizing pulse energy, more than 10 nJ and optimizing pulse duration, pulses as short as 35 fs can be routinely obtained [16].

1.2. Motivation in Synchronization of Laser Oscillators

Passively modelocked lasers generate trains of femtosecond pulses, corresponding to a frequency comb in frequency domain. Although fiber lasers have superior short term stability (above 100 kHz), their long term performance suffers from various effects (i.e. rapid temperature change, pump power instabilities, upper state lifetime of the dopant in gain fiber, etc). This problem can be solved by locking the laser to an RF or microwave reference oscillator, hence improving its short term stability. As the laser pulses are depicted as frequency combs in frequency domain, synchronizing a laser to an ultrastable, but single frequency RF source would automatically turn out to be an ultrastable frequency source not at a single frequency but at discrete frequencies separated by the repetition rate of the laser. Clearly stabilizing a laser to an ultrastable source at particular frequency and getting the desired ultrastable frequency of choice would be much more efficient in every aspect rather than building a second RF source at the choice of frequency.

Chapter 2

Introduction to Nonlinear Optics

Much of ultrafast optics is based on understanding the basics of nonlinearities in optics. This chapter gives basic theories of nonlinear optics, followed by brief descriptions of major optical interactions due to nonlinearity. This chapter is mostly based on [17], further details can be found there.

2.1. Nonlinear Optical Susceptibility

Nonlinear optics emerged with the realization that optical properties of a material changes with light presence. Modification of optical properties in a material requires high intensities of light. At first this phenomenon seemed to be a problem for optical studies, but later became the foundation of laser technology.

The nonlinearity occurs in the sense that the response of a material to applied light is "nonlinear". For example, high harmonic generation processes depends on power of the applied field strengths, i.e. square of the applied field leads to second harmonic generation, cube of the applied field leads to third harmonic generation.

Polarization has a key role in describing nonlinear optics. It shall be examined in section 3.1 that the nonlinear wave equation is,

$$\nabla^2 E - \frac{1}{c^2}\frac{\partial^2 E}{\partial t^2} = \mu_0 \frac{\partial^2 P^{NL}}{\partial t^2} \tag{2.1}$$

where c is the speed of light in vacuum and n is the linear refractive index. One can see from the above equation that whenever $\frac{\partial^2 P^{NL}}{\partial t^2}$ term is nonzero, the charged particles are accelerated and as Larmor's theorem stated, charged particles under acceleration are the source of electromagnetic radiation.

In conventional optics, polarization $P(t)$ of a material depends on the field strength $E(t)$ as;

$$P(t) = \varepsilon_0 \chi^{(1)} E(t) \tag{2.2}$$

where $\chi^{(1)}$ is the linear susceptibility of the material. However, nonlinear response of materials does not satisfy Equation (2.2). The applied field causes anharmonic motion of bound electrons in a material as a result polarization $P(t)$ satisfies the more general relation;

$$P(t) = \varepsilon_0 \left(\chi^{(1)} E(t) + \chi^{(2)} E^2(t) + \chi^{(3)} E^3(t) \dots \right) \tag{2.3}$$

$$\equiv P_{linear} + P_{nonlinear} \tag{2.4}$$

where $\chi^{(2)}$ and $\chi^{(3)}$ are known as the second and third-order nonlinear optical susceptibilities. In these generalized equations (Equations. (2.3) and (2.4)), $\varepsilon_0\chi^{(1)}E(t)$ or P_{linear}, the linear term is the dominant contribution to the overall polarization of the material. Other terms are the correction factors required for compensation of very high applied field effects on polarization. As one might expect, the propagation of light in fiber is ruled by Maxwell's equations from which wave equation is emerged. Nonlinear terms in polarization also transform the wave equation into a nonlinear differential equation which has special solutions (light propagation in fibers will be examined in greater detail in later sections). $\varepsilon_0\chi^{(2)}E(t)$, the second order nonlinear polarization is responsible for effects like *Second-Harmonic Generation* whereas $P^{(3)}(t)$, the third order nonlinear polarization triggers effects like *Kerr Nonlinearity*, both of which will be explained in detail in subsequent sections. $P^{(2)}(t)$ occurs in media with molecular level inversion symmetry (centrosymmetric media), hence it is zero for liquids, gases, amorphous solids(i.e. glass) and most crystals because they have no inversion symmetry. However $P^{(3)}(t)$ can occur both in centrosymmetric and noncentrosymmetric media. This distinction is the reason that in spite of high intensities, there is no second harmonic generation in a laser cavity consisting of only fibers and free-space; and one needs birefringent crystals inside a laser cavity to create second harmonic of the pulse. Similarly it is the reason that weaker polarization term ($P^{(3)}(t)$) has the dominant nonlinear effect in a fiber laser. i.e. Kerr effect.

A simple order of magnitude estimate of susceptibility values might be calculated as follows; the second order polarization term $P^{(2)}(t)$ would be significant enough with respect to linear term $P^{(1)}(t)$ when the amplitude of the applied field strength *E* is on the

order of atomic electric field strength $E_{at}=e/a_o^2$ where e is the electron charge and $a_o=\hbar/me^2$ is the Bohr radius of the hydrogen atom ($\hbar$ is Planck's constant divided by 2π and m is the electron mass). Substituting the values of physical constants $\hbar$, m and e from literature, E_{at} is found to be $6.\widetilde{66} \times 10^6$ m/V. Thus the second-order susceptibility $\chi^{(2)}$ would be on the order of $\chi^{(1)}/ E_{at}$. $\chi^{(1)}$ is almost unity for condensed matter, so $\chi^{(2)}$ value for condensed matter is given as;

$$\chi^{(2)} \approx 2.09 \text{ x } 10^{-11} \text{ m/V} \tag{2.5}$$

Similarly, $\chi^{(3)}$would be on the order of $\chi^{(1)}/ E_{at}^2$, which has a value for condensed matter;

$$\chi^{(3)} \approx 4.2 \text{ x } 10^{-23} \text{ m}^2/\text{V}^2 \tag{2.6}$$

These order of magnitude values of linear susceptibility terms would be a hint why nonlinearity requires high intensities to govern light propagation inside optical media.

2.2.Nonlinear Optical Interactions

In this section a number of nonlinear optical interactions will be introduced briefly and be explained how they can be integrated into Equation (2.3), the general polarization equation. However some of these interactions are beyond the scope of this thesis, hence only the interactions that govern the physics in fiber lasers will be examined in detail in later sections.

Second-Harmonic Generation (SHG):

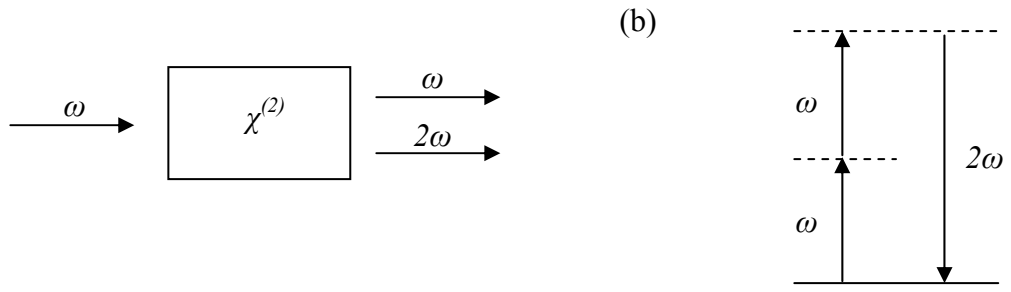

Figure 2.1. (a) Illustration of SHG. (b) Energy-level diagram SHG.

In second-harmonic generation two photons at same frequency ω are vanished and a photon at frequency of 2ω is created in a single quantum mechanical process. This is illustrated in Figure 2.1.a. In Figure 2.1.b, the solid line is the ground state and the dashed lines are the virtual levels, which represent essentially the combined energy of one of the energy eigenstates of the atom and of one or more photons of the radiation field.

In theory a laser beam with electric field;

$$E(t) = Ee^{-i\omega t} + c.c. \tag{2.7}$$

is incident upon a crystal with a nonzero second order susceptibility $\chi^{(2)}$ then the nonlinear polarization that is created in such a crystal is given as;

$$P^{(2)}(t) = \varepsilon_0\chi^{(2)}E^2(t) = 2\varepsilon_0\chi^{(2)}EE^* + \left(\varepsilon_0\chi^{(2)}E^2e^{-2\omega t} + c.c.\right) \tag{2.8}$$

In Equation 2.8, the second-order polarization consists of a contribution at zero frequency and a contribution at frequency 2ω. According to Equation (2.1), the nonlinear wave equation, contribution at frequency 2ω leads to the generation of radiation at the second-harmonic frequency. However contribution at zero frequency cannot lead to the generation of any electromagnetic radiation because its second time derivative is zero.

Sum-Frequency Generation (SFG):

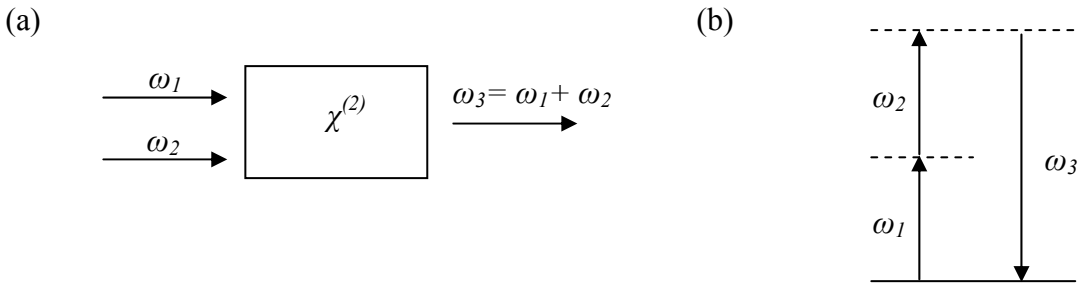

Figure 2.2. (a) Illustration of SFG. (b) Energy-level diagram SFG

Sum-frequency generation is analogous to that of second-harmonic generation, except that in SFG the two input frequencies are different as in Figure 2.2.a. If a laser beam with electric field *E(t)* (Equation (2.7)) is incident upon a crystal with nonzero $\chi^{(2)}$, the nonlinear polarization that is created in SFG process is given by;

$$P(\omega_1 + \omega_2) = 2\varepsilon_0 \chi^{(2)} E_1 E_2 \tag{2.9}$$

Difference-Frequency Generation (DFG):

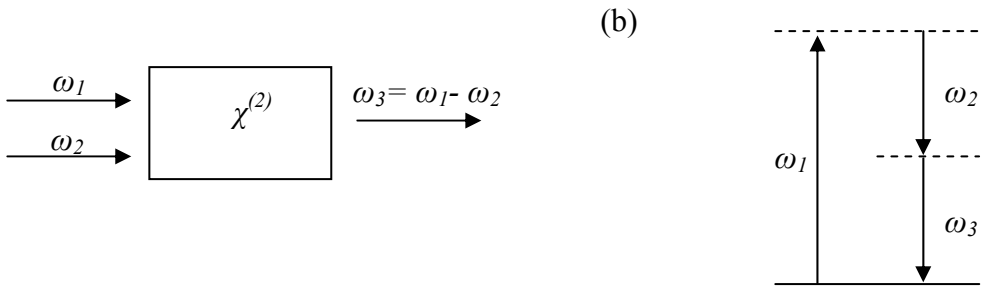

Figure 2.3. (a) Illustration of DFG. (b) Energy-level diagram DFG

In difference-frequency generation, difference frequency of applied fields is generated (Figure 2.3). The process is described by the nonlinear polarization;

$$P(\omega_1 - \omega_2) = 2\varepsilon_0 \chi^{(2)} E_1 E_2^* \tag{2.10}$$

To consider the general picture of second order frequency generation, assume an optical field with electric field;

$$E(t) = Ee^{-i\omega_1 t} + Ee^{-i\omega_2 t} + c.c. \tag{2.11}$$

is incident upon a nonlinear medium with nonzero $\chi^{(2)}$. Then the nonlinear polarization created in such a medium is of the form;

$$P^{(2)}(t) = \varepsilon_0 \chi^{(2)}[E_1^2 e^{-2i\omega_1 t} + E_2^2 e^{-2i\omega_2 t} + 2E_1 E_2 e^{-i(\omega_1+\omega_2)t} + 2E_1 E_2^* e^{-i(\omega_1-\omega_2)t}$$

$$+c.c] + 2\varepsilon_0 \chi^{(2)}[E_1 E_1^* + E_2 E_2^*] \quad (2.12)$$

Each of the complex amplitude term of various frequency components of this nonlinear polarization corresponds to different nonlinear process. First two terms would be the SHG form, third one is the SFG form and the last one is the DFG form. However, one should note that no more than one of these frequency components will be present with any appreciable intensity in the radiation generated by the nonlinear optical medium. The reason is that nonlinear polarization processes can produce decent output signal only if a certain phase-matching condition is satisfied.

Third-Order Polarization:

Third-order contribution to the nonlinear polarization in a nonlinear media with nonzero $\chi^{(3)}$ is;

$$P^{(3)}(t) = \varepsilon_0 \chi^{(3)} E^3(t) \quad (2.13)$$

For the general picture, an applied electric field consisting three frequency components is assumed to be incident upon the nonlinear media;

$$E(t) = Ee^{-i\omega_1 t} + Ee^{-i\omega_2 t} + Ee^{-i\omega_3 t} + c.c. \quad (2.14)$$

However in this case calculated $E^3(t)$ contains 44 different frequency components corresponding to distinct mixing processes, hence the expression for $P^3(t)$ will be very complicated. For the purpose of simplicity and sufficiency, the simple case in which the applied field is in single frequency is considered;

$$E(t) = \mathcal{E}cos\omega t \tag{2.15}$$

Through the use of the trigonometric identity, $cos^3\omega t = \frac{1}{4}cos3\omega t + \frac{3}{4}cos\omega t$, the nonlinear polarization can be found as;

$$P^{(3)}(t) = \frac{1}{4}\varepsilon_0\chi^{(3)}\mathcal{E}^3cos3\omega t + \frac{3}{4}\varepsilon_0\chi^{(3)}\mathcal{E}^3cos\omega t \tag{2.16}$$

In Equation (2.16) each term corresponds to a different nonlinear process which will be briefly introduced below.

Third-Harmonic Generation (THG):

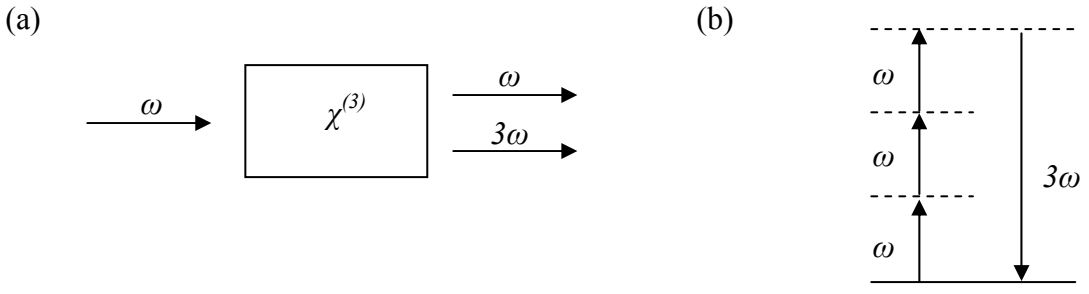

Figure 2.4. (a) Illustration of THG. (b) Energy-level diagram THG

The first term in Equation (2.16) describes a nonlinear response at frequency 3ω created by an applied field at frequency ω. This term defines the process of third-harmonic generation, which is described in Figure 2.4. In this process three photons at frequency ω are destroyed and one photon at frequency 3ω is created in a single quantum mechanical process.

Intensity-Dependent Refractive Index:

The second term in Equation 2.16 describes a nonlinear contribution to the polarization at the frequency of the incident field ω. Hence it leads to a nonlinear contribution to the refractive index experienced by the incident field at frequency ω. The nonlinear refractive index can be represented as;

$$n = n_0 + n_2 I \tag{2.17}$$

where $n_0$is the linear refractive index and

$$n_2 = \frac{3}{8n} Re(\chi^{(3)}_{xxxx}) \tag{2.18}$$

is an optical constant that decides the strength of the optical nonlinearity and where

$$I = n_2 |E|^2 \tag{2.19}$$

is the intensity of the incident field.

This process is also known as *Kerr nonlinearity* which plays an important role in fiber lasers.

All of the processes described up to this point are examples of parametric processes. In parametric processes the initial and final quantum mechanical states of the system are same. Conversely, processes in which the initial and final quantum mechanical states are distinct real levels are known as nonparametric processes. Mainly two differences are there between parametric and nonparametric processes. The former one is always described by a real susceptibility, whereas the latter can be described by a complex susceptibility. The second difference is that photon energy is conserved in a parametric process; conversely photon energy need not be conserved in a nonparametric process. The following two nonlinear processes are examples of nonparametric processes.

Saturable Absorption:

Many materials' absorption coefficient decreases when measured using high intensity lasers. The dependence of the measured absorption coefficient α on the intensity I of the incident field is given by;

$$\alpha = \frac{\alpha_0}{1 + I/I_s} \tag{2.20}$$

where α_0 is the low-intensity absorption coefficient and I_s is the saturation intensity.

Saturable absorption is one of the key concepts in mode-locking of lasers hence its role in laser operation will be described in detail in Section 3.3.

Two-Photon Absorption:

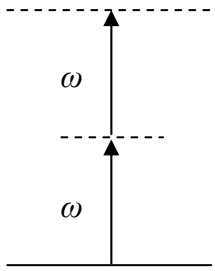

Figure 2.5. Energy-level diagram of two-photon absorption.

In two-photon absorption (illustrated in Figure 2.5) an atom has a transition from its ground state to an exited state by the simultaneous absorption of two photons. In contrast with linear optics, the absorption coefficient that describes two-photon absorption increases linearly with laser intensity as;

$$\sigma = \sigma^{(2)} I \tag{2.21}$$

where $\sigma^{(2)}$ is a coefficient that describes two-photon absorption. In addition, the atomic transition rate R due to two-photon absorption is proportional to the square of the field intensity, since $R = \sigma I/\hbar\omega$, or to;

$$R = \frac{\sigma^{(2)} I^2}{\hbar\omega} \tag{2.22}$$

Stimulated Raman Scattering:

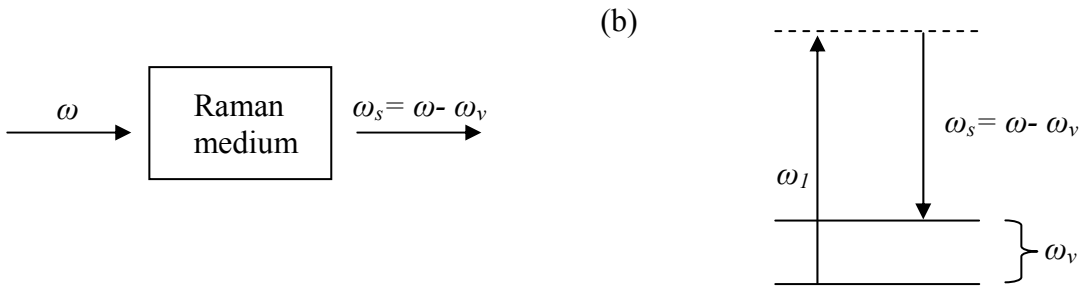

Figure 2.6. Illustration and energy-level diagram of stimulated Raman scattering.

In stimulated Raman scattering (illustrated in Figure 2.6) a photon at frequency ω vanishes and a photon at the Stokes frequency $\omega_s = \omega - \omega_v$ forms. In this picture ω_v is the frequency that the atom is left in an excited state with energy $\hbar\omega_v$ after the scattering. The stimulated Raman scattering process is very efficient compared to normal or spontaneous Raman scattering where both an exited atom's vibration and a photon is annihilated to have a photon at the anti-Stokes shifted frequency $\omega_s = \omega + \omega_v$

Chapter 3

Theory of Fiber Lasers

To understand and describe the propagation of laser light in a dispersive optical medium, it is necessary to take the theory of electromagnetic wave propagation into account. This chapter gives derivation of basic wave equation, followed by the theory of pulse propagation in dispersive optical medium. Discussion of amplification in fibers and mode-locking will conclude the section. This chapter is mostly based on [18,19], further details can be found there.

3.1. Ultra-short Pulse Propagation in Fibers

Like all electromagnetic phenomena, the propagation of pulses in optical fibers is ruled by Maxwell's equations;

$$\nabla . \boldsymbol{D} = \rho \tag{3.1}$$

$$\nabla . \boldsymbol{B} = 0 \tag{3.2}$$

$$\nabla \times \boldsymbol{E} = -\frac{\partial \boldsymbol{B}}{\partial t} \tag{3.3}$$

$$\nabla \times \boldsymbol{H} = \boldsymbol{j} + \frac{\partial \boldsymbol{D}}{\partial t} \tag{3.4}$$

where $\boldsymbol{B}$ and $\boldsymbol{D}$ are magnetic and electric flux densities, respectively, and $\boldsymbol{H}$ and $\boldsymbol{E}$ are the corresponding magnetic and electric field vectors. Since there are no free charges in optical fibers, free charges ρ and current density $\boldsymbol{j}$ vanish. The flux densities are related to electric and magnetic field through the relations given by;

$$\boldsymbol{D} = \varepsilon_0 \boldsymbol{E} + \boldsymbol{P} \tag{3.5}$$

$$\boldsymbol{B} = \mu_0 \boldsymbol{H} + \boldsymbol{M} \tag{3.6}$$

Where ε_0 is the vacuum permittivity, μ_0 is the vacuum permeability, and $\boldsymbol{P}$ and $\boldsymbol{M}$ are induced electric and magnetic polarizations respectively. For an optical medium $\boldsymbol{M}$ is zero. Using the mathematical identity $\nabla \times (\nabla \times \boldsymbol{A}) = \nabla(\nabla . \boldsymbol{A}) - \nabla^2 \boldsymbol{A}$ and taking the curl of both sides of Equation (3.3) gives;

$$\nabla(\nabla . \boldsymbol{E}) - \nabla^2 \boldsymbol{E} = -\frac{\partial}{\partial t}(\nabla \times \boldsymbol{B}) \tag{3.7}$$

Using Equations (3.4), (3.5) and (3.6) one can obtain;

$$\nabla \times \boldsymbol{B} = \mu_0 \varepsilon_0 \frac{\partial \boldsymbol{E}}{\partial t} + \mu_0 \frac{\partial \boldsymbol{P}}{\partial t} \tag{3.8}$$

Substituting Equation (3.8) in (3.7) gives an equation depending on $\boldsymbol{E}$ and $\boldsymbol{P}$ only;

$$\nabla(\nabla . \boldsymbol{E}) - \nabla^2 \boldsymbol{E} = -\mu_0 \varepsilon_0 \frac{\partial^2 \boldsymbol{E}}{\partial t^2} - \mu_0 \frac{\partial^2 \boldsymbol{P}}{\partial t^2} \tag{3.9}$$

Since there are no free charge carriers, $\nabla . \boldsymbol{E} = 0$ and using the relation $\mu_0 \varepsilon_0 = 1/c^2$, Equation (3.9) can be reduced to the wave equation;

$$\nabla^2 \boldsymbol{E} - \frac{1}{c^2}\frac{\partial^2 \boldsymbol{E}}{\partial t^2} = \mu_0 \frac{\partial^2 \boldsymbol{P}}{\partial t^2} \tag{3.10}$$

A few assumptions need to be made before solving Equation (3.10). First the nonlinearity in $\boldsymbol{P}$ is treated as a small perturbation. Second, the optical field maintains its polarization along the fiber length so that a scalar approach is valid. Third, the polarization response of the field is instantaneous. This is valid for a nonlinear response that is electronic in nature, since the reconfiguration time of the electron cloud is significantly smaller than the period of the optical light wave. The contributions of molecular vibrations to the nonlinear part of the polarization (the Raman effect) is neglected for now and will be discussed later in this section.

The third assumption lets the expansion of the induced polarization in a series of powers of instantaneous electric field;

$$\boldsymbol{P}(\boldsymbol{r},t) = \varepsilon_0\big(\underbrace{\chi^{(1)}\boldsymbol{E}(\boldsymbol{r},t)}_{\boldsymbol{P}_L} + \underbrace{\chi^{(2)}\boldsymbol{E}^2(\boldsymbol{r},t) + \chi^{(3)}\boldsymbol{E}^3(\boldsymbol{r},t)\ldots}_{\boldsymbol{P}_{NL}}\big) = \boldsymbol{P}_L + \boldsymbol{P}_{NL} \tag{3.11}$$

The electric field has a time structure that has a rapidly and slowly varying component. The slow timescale is the width of the pulse, which is typically on the order of 100 fs. The fast timescale is the optical cycle, which is on the order of $\lambda/c \approx 5$ fs. Hence it is useful to separate the timescales of electric field and polarization components in the form;

$$\boldsymbol{E}(\boldsymbol{r},t) = \frac{1}{2}\boldsymbol{x}[E(\boldsymbol{r},t)\exp(i\beta_0 z - i\omega_0 t) + c.c.] \tag{3.12}$$

$$= \frac{1}{2}\boldsymbol{x}[F(x,y)A(z,t)\exp(i\beta_0 z - i\omega_0 t) + c.c.] \tag{3.13}$$

$$\boldsymbol{P}_L(\boldsymbol{r},t) = \frac{1}{2}\boldsymbol{x}[P_L(\boldsymbol{r},t)\exp(i\beta_0 z - i\omega_0 t) + c.c.] \tag{3.14}$$

$$\boldsymbol{P}_{NL}(\boldsymbol{r},t) = \frac{1}{2}\boldsymbol{x}[P_{NL}(\boldsymbol{r},t)\exp(i\beta_0 z - i\omega_0 t) + c.c.] \tag{3.15}$$

Only the real part of the above equations is physically relevant, hence complex conjugate parts will not be stated anymore. Here, $\boldsymbol{x}$ is the unit vector perpendicular to the propagation direction, which can be ignored because of the assumption that the polarization is maintained during the propagation through the fiber. $E(\boldsymbol{r},t)$ and $P_{L/NL}(\boldsymbol{r},t)$ are the slowly varying envelopes of the corresponding components. For future simplifications, the dependencies on x and y (modal pattern) from that on z and t (propagation) are separated. This is appropriate because the transverse mode structure in the fiber is to first order independent of propagation length and time. The quickly varying parts in both z and t are expressed as a plane wave which propagates in the z-direction and is of definite frequency ω_0 and associated wave number $\beta_0 = n\omega_0/c$.

The assumption in Equation (3.11) lead to the approximation of nonlinear polarization [18]

$$\boldsymbol{P}_{NL}(\boldsymbol{r},t) = \varepsilon_0 \varepsilon_{NL}(\boldsymbol{r},t)E(\boldsymbol{r},t) \tag{3.16}$$

where the nonlinear contribution to the dielectric constant is defined as;

$$\varepsilon_{NL}(\boldsymbol{r},t) = \frac{3}{4}\chi^{(3)}|E(\boldsymbol{r},t)|^2 \tag{3.17}$$

To obtain the wave equation for the slowly varying amplitude $E(\boldsymbol{r},t)$ it is useful to work in the Fourier domain. However, because ε_{NL} is intensity dependent, it is not possible to apply a Fourier transform. In the subsequent approach perturbative assumption of $\boldsymbol{P}_{NL}$ is used, hence ε_{NL} can be treated as locally constant. Substituting Equations (3.12) through (3.15) in Equation (3.10), the Fourier transform $\tilde{E}(r,\omega-\omega_0)$, defined as;

$$\tilde{E}(\boldsymbol{r},\omega-\omega_0) = \int_{-\infty}^{\infty} E(\boldsymbol{r},t)\exp[i(\omega-\omega_0)t]dt \tag{3.18}$$

is found to satisfy the Helmholtz equation;

$$\left(\nabla^2 + \varepsilon_{NL}(\boldsymbol{r},\omega)\frac{\omega^2}{c^2}\right)\tilde{E}(\boldsymbol{r},\omega) = 0 \tag{3.19}$$

with the dielectric function given by

$$\varepsilon(\omega) = 1 + \varepsilon_L + \varepsilon_{NL} \tag{3.20}$$

Equation (3.19) can be solved by using the method of separation of variables. A solution of the form;

$$\tilde{E}(\boldsymbol{r},\omega-\omega_0) = F(x,y)\tilde{A}(z,\omega-\omega_0)\exp(ik_0 z) \tag{3.21}$$

which is the Fourier transform of Equation (3.13), is assumed; where $\tilde{A}(z,\omega)$ is a slowly varying function of z and $F(x,y)$ is the modal distribution of the pulse in the fiber. Further calculations (see [18] for details) leads to two equations for $F(x,y)$ and $\tilde{A}(z,\omega)$;

$$\frac{\partial^2 F}{\partial x^2}+\frac{\partial^2 F}{\partial y^2}+\left[\varepsilon(\omega)\frac{\omega^2}{c^2}-\tilde{\beta}^2(\omega)\right]F=0 \tag{3.22}$$

$$2i\beta_0\frac{\partial \tilde{A}}{\partial z}+\left(\tilde{\beta}^2(\omega)-\beta_0^2\right)\tilde{A}=0 \tag{3.23}$$

$\tilde{A}(z,\omega)$ is assumed to be a slowly varying function of z, its second derivative was neglected. The wave number $\beta(\omega)$ is determined by solving the eigenvalue equation for the fiber modes (see [18] for details). The dielectric function $\varepsilon(\omega)$ in Equation (3.22) is approximated by;

$$\varepsilon(\omega)=(n(\omega)+\Delta n)^2\approx n^2+2n\Delta n \tag{3.24}$$

where Δn is a small perturbation given by the nonlinearity of the refractive index and the absorption $\tilde{\alpha}$ and gain $\tilde{g}$ in the fiber;

$$\Delta n=n_2|E|^2+\frac{i\tilde{\alpha}(\omega)-\tilde{g}(\omega)}{2k_0} \tag{3.25}$$

The solution for the modal distribution $F(x,y)$ is not affected compared to the case without the perturbation. However, the eigenvalue solution becomes;

$$\tilde{\beta}(\omega) = \beta(\omega) + \Delta\beta(\omega) \tag{3.26}$$

$$\Delta\beta(\omega) = \frac{\omega^2 n(\omega)}{c^2 \beta(\omega)} \frac{\int\int_{-\infty}^{\infty} \Delta n(\omega) |F(x,y)|^2 dxdy}{\int\int_{-\infty}^{\infty} |F(x,y)|^2 dxdy} \tag{3.27}$$

Only single-mode fibers are considered here, $F(x,y)$ corresponds to the modal distribution of the fundamental fiber mode HE_{11} given by [18]

$$F(x,y) = J_0(p\rho), \quad \rho = \sqrt{x^2 + y^2} \leq a \tag{3.28}$$

inside the core and;

$$F(x,y) = \sqrt{a/\rho} J_0(p\rho) \exp[-q(\rho - a)], \quad \rho \geq a \tag{3.29}$$

outside the core. This modal distribution is cumbersome in practice, is approximated by the Gaussian distribution;

$$F(x,y) = \exp[-(x^2 + y^2)/w^2] \tag{3.30}$$

where the width parameter w is obtained by curve fitting.

Rewriting Equation (3.23) by using (3.26) and approximating $\tilde{\beta}^2(\omega) - \beta_0^2$ by $2\beta_0(\tilde{\beta}^2(\omega) - \beta_0)$ gives;

$$\frac{\partial \tilde{A}}{\partial z} = i[\beta(\omega) + \Delta\beta(\omega) - \beta_0]\tilde{A} \tag{3.31}$$

After this point, one can go back to the time domain by taking the inverse Fourier transform of Equation (3.31), and obtain the slowly varying envelope function $A(z,t)$. Since an exact functional form for $\beta(\omega)$ is not known, it is useful to expand it in a Taylor series around the carrier frequency ω_0 as;

$$\beta(\omega) = \beta_0 + (\omega - \omega_0)\beta_1 + \frac{1}{2}(\omega - \omega_0)^2\beta_2 + \frac{1}{6}(\omega - \omega_0)^3\beta_3 + \cdots \tag{3.32}$$

where $\beta_0 \equiv \beta(\omega_0)$ and,

$$\beta_n = \left.\frac{d^n\beta}{d\omega^n}\right|_{\omega=\omega_0} \quad (m = 1,2,\dots) \tag{3.33}$$

The cubic and higher-order terms in the expansion are negligible it the pulse duration in the ps-range. For femtosecond pulses however, third-order dispersion has to be taken into account. Using a similar expansion for $\Delta\beta(\omega)$, substituting both expansions in Equation (3.31) and taking the inverse Fourier transform it by using;

$$A(z,t) = \frac{1}{2\pi}\int_{-\infty}^{\infty} \tilde{A}(z,\ \omega - \omega_0)\exp[-i(\omega - \omega_0)t]\,\mathrm{d}\omega \tag{3.34}$$

gives the resulting equation for $A(z,t)$;

$$\frac{\partial A}{\partial z} + \beta_1\frac{\partial A}{\partial t} + \frac{i\beta_2}{2}\frac{\partial^2 A}{\partial t^2} = i\Delta\beta_0 A \tag{3.35}$$

The effect of fiber loss and nonlinearity is included in the term $\Delta\beta_0$ and can be evaluated using Equation (3.27). Using $\beta(\omega) \approx n(\omega)\omega/c$ and assuming $F(x,y)$ in (3.27) does not change much over the pulse bandwidth lead to;

$$\frac{\partial A}{\partial z} + \beta_1 \frac{\partial A}{\partial t} + \frac{i\beta_2}{2}\frac{\partial^2 A}{\partial t^2} + \frac{\alpha}{2}A = i\gamma(\omega_0)|A|^2 A \tag{3.36}$$

with the nonlinear parameter γ defined as;

$$\gamma = \frac{n_2(\omega_0)\omega_0}{cS_{eff}} \tag{3.37}$$

where S_{eff} is the effective mode area of an optical fiber. Evaluation of it requires the use of the modal distribution $F(x,y)$. If $F(x,y)$ is approximated by a Gaussian distribution, $S_{eff} = \pi w^2$. Typically, S_{eff} ranges between 1-100 μm^2 in the 1.5 μm region.

A transformation of Equation (3.36) into a reference frame moving at the group velocity $v_g = 1/\beta_1$ of the pulse envelope leads to;

$$\frac{\partial A}{\partial z} + \frac{i\beta_2}{2}\frac{\partial^2 A}{\partial T^2} + \frac{\alpha}{2}A = i\gamma(\omega_0)|A|^2 A \tag{3.38}$$

where $T = t - \frac{z}{v_g} \equiv t - \beta_1 z$. Because of resemblance this equation is called the nonlinear Schrödinger equation (NLSE) and is used to describe the propagation of ps-range pulses through optical fibers, taking into account chromatic dispersion by β_2, fiber losses by α and fiber nonlinearities by γ.

It is useful to introduce two length scales, *dispersion length* L_D and *nonlinear length* L_{NL}. This makes it possible to compare the relative strengths of effects over the propagation distance. These *lengths* are defined as;

$$L_D = \frac{T_0^2}{\beta_2}, \qquad L_{NL} = \frac{1}{\gamma P_0} \tag{3.39}$$

Here T_0 is the initial pulse length and P_0 is the pulse peak power. Rewriting equation 2.29 with these new parameters leads to;

$$\frac{\partial a}{\partial z} + \frac{i}{2}\frac{L}{L_D}\frac{\partial^2 a}{\partial \tau^2} + \frac{\alpha}{2}a = i\frac{L}{L_{NL}}|a|^2 a \tag{3.40}$$

where the absolute square of the field now gives power instead of intensity, through the transformation $a(z,\tau) = A(z,t)/\sqrt{S_{eff}}$.

Unfortunately, some of the assumptions used in deriving the NLSE are not valid for ultra-short pulses (100 fs regime). The bandwidth needed to support such short pulses is so large that third-order dispersion effects can no longer be neglected. Furthermore the assumption that the fiber nonlinearity responds instantaneously compared to the pulse duration is no longer supported. In addition, the contribution to $\chi^{(3)}$ from the Raman effect becomes significant, as it occurs over a time scale of around 60 fs. The next few pages in this section will deal with the extension of the NLSE to include these effects.

For pulses with a wide spectrum, the Raman effect can amplify low-frequency components of a pulse by energy transfer from the high-frequency components of the same pulse. As a

result of it, a red-shift of the optical spectrum of the pulse, a feature referred to as *Raman-induced frequency shift* takes place. To include this effect, one needs to re-evaluate the nonlinear polarization equation (3.10). Any $\chi^{(2)}$ related effects are still neglected as they require phase-matching. The scalar form of nonlinear polarization is given by;

$$P_{NL}(\boldsymbol{r},t) = \frac{3\varepsilon_0}{4}\chi^{(3)}_{xxxx}E(\boldsymbol{r},t)\int_{-\infty}^{t} R(t-t_1)|E(\boldsymbol{r},t_1)|^2 dt_1 \tag{3.41}$$

which includes the nonlinear effects in a response function $\chi^{(3)}R(t-t_1)$ where $R(t)$ is defined similarly to a time-delayed delta function such that $\int_{-\infty}^{\infty} R(t)dt = 1$.This corresponds to $R(t-t_1) = \delta(t-(t_1+\Delta t))$. The upper limit of integration extends up to t to ensure causality. Somewhat lengthy algebra leads to the expression (see [18] for details);

$$\frac{\partial A}{\partial z} + \beta_1\frac{\partial A}{\partial t} + \frac{i\beta_2}{2}\frac{\partial^2 A}{\partial t^2} - \frac{\beta_3}{6}\frac{\partial^3 A}{\partial t^3} + \frac{1}{2}\left(\alpha + i\alpha_1\frac{\partial}{\partial t}\right)A$$

$$= i\left(\gamma + i\gamma_1\frac{\partial}{\partial t}\right)\left(A(z,t)\int_0^{\infty} R(t')|A(z,t-t')|^2\right) \tag{3.42}$$

For pulse durations that can contain many optical cycles (pulse width $>$ 100 fs), it is possible to simplify Equation (3.42) by setting $\alpha_1 = 0$ and $\gamma_1 = \gamma/\omega_0$ and using a Taylor expansion of the form;

$$|A(z,t-t')|^2 \approx |A(z,t)|^2 - t'\frac{\partial}{\partial t}|A(z,t)|^2 \tag{3.43}$$

The following equation is acquired;

$$\frac{\partial A}{\partial z}+\frac{\alpha}{2}A+\frac{i\beta_2}{2}\frac{\partial^2 A}{\partial t^2}-\frac{\beta_3}{6}\frac{\partial^3 A}{\partial t^3}=i\gamma\left[|A|^2A+\frac{i}{\omega_0}\frac{\partial}{\partial T}(|A|^2A)-T_RA\frac{\partial|A|^2}{\partial T}\right] \quad (3.44)$$

where a reference frame moving with the group velocity is used similar to the case in Equation (3.38). T_R is defined as the first moment of the nonlinear response function $T_R=\int_{-\infty}^{\infty}tR(t)dt$. This latest form of the NLSE also contains the third-order dispersion (β_3 term), the effect of self-steepening (ω_0^{-1} term) caused by the intensity dependence of the group velocity and the Raman-induced frequency shift (T_R term) caused by the delayed Raman response. A numerical value has been deduced experimentally as $T_R=3$ fs for the spectral region around 1550 nm.

Solution of the NLSE is pretty straight-forward for negative β_2. For this case, the solution does not change along the fiber length. Such a phenomenon is called a solitary wave solution. It was first observed in 1834 by Scott Russell in water waves propagating with undistorted phase over several kilometers through a canal.

The physical origin for optical solitons is a balance of dispersion and nonlinearity. Equation (3.38) can be rewritten as;

$$\frac{\partial A}{\partial z}=i\gamma(\omega_0)|A|^2A-\frac{i\beta_2}{2}\frac{\partial^2 A}{\partial T^2} \quad (3.45)$$

with the assumption of no fiber losses ($\alpha = 0$). If both β_2 and $\frac{\partial^2 A}{\partial T^2}$ are negative, there can be a combination of pulse duration (the parameter responsible for the magnitude of β_2) and pulse energy (the parameter responsible for magnitude of γ), such that both terms cancel and $\frac{\partial A}{\partial z} = 0$. This means that, the envelope of the pulse does not change while propagating through a fiber if fiber losses and higher order nonlinear effects are neglected. The solution is characterized by a hyperbolic secant pulse shape;

$$|A(t)| = \sqrt{\frac{|\beta_2|}{\gamma T_0^2}} \operatorname{sech}\left(\frac{T}{T_0}\right) \tag{3.46}$$

3.2. Amplification in Rare-Earth Doped Fibers

Optical fibers can amplify light at correct wavelength through stimulated emission. This is done by optically pumping the amplifier fiber to obtain population inversion. Depending on the energy levels of the dopants (rare-earth elements like erbium, ytterbium, neodymium, samarium and thulium), lasing schemes can be classified as a three- or four-level scheme (Figure 3.1). In either case, dopants absorb pump photons to reach an excitation stage than relax rapidly into a lower-energy excited state. The life time of this intermediate state is usually long (around 10ms for erbium and 1ms for ytterbium), and the stored energy is used to amplify incident light through stimulated emission. The difference between the three- and four-level lasing schemes is the energy state to which the dopant relaxes after each stimulated-emission event. In the case of a three-level lasing scheme, the dopant ends up in the ground state, whereas it occupies an exited state in the case of a four-level lasing scheme. Erbium-doped fiber lasers and amplifiers make use of three-level scheme.

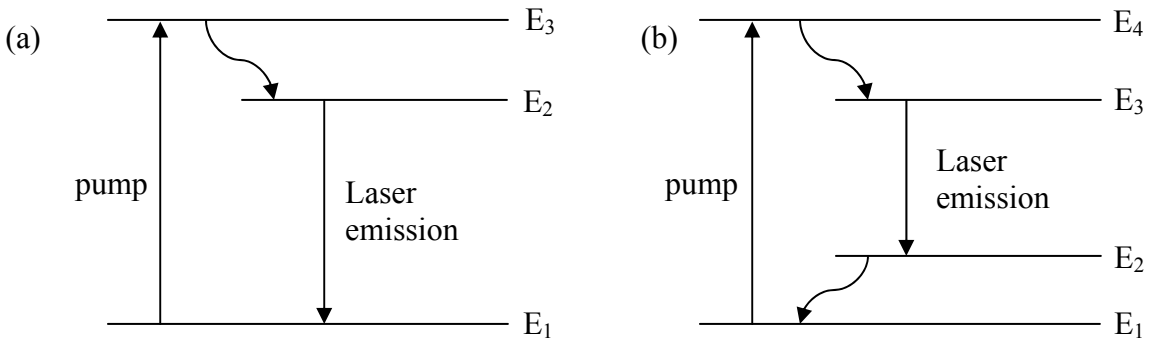

Figure 3.1. Illustration of (a) three-and (b) four-level lasing schemes

Optical pumping creates the necessary population inversion between two energy states and provides the optical gain. Using the appropriate rate equations (see [20] for details), the gain coefficient for a homogeneously broadened gain medium can be written as;

$$g(\omega) = \frac{g_0}{1 + (\omega - \omega_a)^2 T_2^2 + P/P_s} \tag{3.47}$$

where g_0 is the peak gain value, ω is the frequency of the incident signal, ω_a is the atomic transition frequency and P is the optical power of the signal being amplified. The saturation power P_s is mainly influenced by the parameters such as the fluorescence time T_1 (in the range of 1 μs to 10 ms for commonly used dopants) and the transition cross section σ. The parameter T_2 is the dipole relaxation time and is usually on the order of 0.1 ps for fiber amplifiers.

If the saturation effect is neglected in Equation (3.47), the gain reduction for frequencies off the transition frequency is governed by a Lorentzian profile. The gain bandwidth Δv is

defined as the full width at half maximum (FWHM) of the gain spectrum $g(\omega)$, given for a Lorentzian spectrum as;

$$\Delta v_g = \frac{\Delta\omega_g}{2\pi} = \frac{1}{\pi T^2} \tag{3.48}$$

However, the actual gain spectrum of a fiber laser can deviate significantly from the Lorentzian profile. The shape and the width of the gain spectrum are sensitive to core composition (i.e. the amorphous nature of the silica and the presence of other co-dopants such as aluminum or germanium).

In the latter part of this section, the effects of gain provided by dopants for the NLSE will be examined.

The lasing process can be approximated by a two-level system, as the lifetime of the first upper state is significantly shorter than the lifetime of the state from which stimulated emission takes place. The dynamic response of a two-level system is governed by the Maxwell-Bloch equations [20]. The starting point is the wave equation (3.10), but the induced polarization $\boldsymbol{P}(\boldsymbol{r})$ has to include a third term $\boldsymbol{P}_d(\boldsymbol{r})$ representing the contribution of dopants. Using the slowly varying envelope approximation similar to Equation (3.14);

$$\boldsymbol{P}_d(\boldsymbol{r},t) = \frac{1}{2}\boldsymbol{x}[P_d(\boldsymbol{r},t)\exp(i\beta_0 z - i\omega_0 t) + c.c.] \tag{3.49}$$

The slowly varying part is dictated by the Bloch [20] equations which relate the population inversion density $W = N_2 - N_1$ to the polarization and electric field;

$$\frac{\partial P(\boldsymbol{r},t)}{\partial t} = -\frac{P(\boldsymbol{r},t)}{T_2} - i(\omega_a - \omega_0)P(\boldsymbol{r},t) - \frac{i\mu^2}{\hbar}E(\boldsymbol{r},t)W \tag{3.50}$$

$$\frac{\partial W}{\partial t} = \frac{W_0 - W}{T_1} - \frac{1}{\hbar}\mathrm{Im}\big(E^*(\boldsymbol{r},t).P(\boldsymbol{r},t)\big) \tag{3.51}$$

where μ is the magnetic dipole moment, ω_a is the atomic transition frequency, and $E(\boldsymbol{r},t)$ is the slowly varying amplitude defined as in Equation (3.14).

Following the same method in previous section for the derivation of NLSE, the NLSE (3.36) is modified as;

$$\frac{\partial A}{\partial z} + \beta_1\frac{\partial A}{\partial t} + \frac{i\beta_2}{2}\frac{\partial^2 A}{\partial t^2} + \frac{\alpha}{2}A = i\gamma(\omega_0)|A|^2A + \frac{i\omega_0}{2\varepsilon_0 c}\langle P_d(\boldsymbol{r},t)\rangle \tag{3.52}$$

where the angled brackets denote an averaging over the mode profile $|F(x,y)|^2$. The preceding three equations (3.50)-(3.52) need to be solved for pulses of a duration comparable to the relaxation time (0.1 ps). The analysis is simplified considerably for longer pulses, where the dopants respond so fast that the induced polarization follows the optical field adiabatically (see [20] for details). Dispersive effects can be included by working in the Fourier domain and defining the dopant susceptibility as;

$$\tilde{P}(\boldsymbol{r},\omega) = \varepsilon_0\chi_d(\boldsymbol{r},\omega)\tilde{E}(\boldsymbol{r},\omega) \tag{3.53}$$

The susceptibility is found [20] as;

$$\chi_d(\boldsymbol{r},\omega) = \frac{\sigma_s W(\boldsymbol{r}) n_0 c/\omega_0}{(\omega-\omega_a)T_2 + i} \tag{3.54}$$

Similar approach used in deriving in NLSE can be performed, provided the dielectric constant is modified to take χ_d into account. This leads to a change in Equation (3.25);

$$\Delta n = n_2|E|^2 + \frac{\chi_d}{2n} \tag{3.55}$$

The major difference is that $\Delta\beta$ in Equation (3.27) becomes frequency dependent due to χ_d. Hence, when transforming the optical field back to the time domain, both β and $\Delta\beta$ must be expanded into a Taylor series. The resulting equation is found after somewhat lengthy algebra (see [21] for details);

$$\frac{\partial A}{\partial z} + \beta_1^{eff}\frac{\partial A}{\partial t} + \frac{i}{2}\beta_2^{eff}\frac{\partial^2 A}{\partial t^2} + \frac{\alpha}{2}A = i\gamma(\omega_0)|A|^2 A + \frac{g_0}{2}\frac{1+i\delta}{1+\delta^2}A \tag{3.56}$$

where

$$\beta_1^{eff} = \beta_1 + \frac{g_0 T_2}{2}\left[\frac{1-\delta^2+2i\delta}{(1+\delta^2)^2}\right] \tag{3.57}$$

$$\beta_2^{eff} = \beta_2 + \frac{g_0 T_2}{2}\left[\frac{\delta(\delta^2-3)+i(1-3\delta^2)}{(1+\delta^2)^3}\right] \tag{3.58}$$

and the detuning parameter $\delta = (\omega_0 - \omega_a)T_2$. The gain g_0 is given by;

$$g_0(z,t) = \frac{\sigma_s \int\int_{-\infty}^{\infty} W(\boldsymbol{r},t)|F(x,y)|^2 dxdy}{\int\int_{-\infty}^{\infty}|F(x,y)|^2 dxdy} \tag{3.59}$$

Spatial averaging is due to the use of Equation (3.55) in (3.27). Equation (3.56) shows that gain not only affects the group velocity of the pulse ($v_g = \beta_1^{-1}$), but also the chromatic dispersion through the effective β_2. The change in the group velocity is usually negligible, since the second term is smaller on the order of 10^{-4} compared to β_1. In contrast, not so for β_2^{eff} since near the zero-dispersion wavelength of the optical fiber, the two terms can become comparable. Even in the special case of $\beta = 0$, β_2^{eff} does not reduce to β_2, in fact it comes down to;

$$\beta_2^{eff} = \beta_2 + ig_0T_2^2 \tag{3.60}$$

which is a complex parameter caused by the gain induced by the dopants. The physical origin of this contribution is called *gain dispersion* which is due to the finite gain bandwidth of doped fibers. Equation (3.60) is a result of the parabolic-gain approximation used in the derivations in [21].

The integration of Equation (3.59) is difficult since the inversion profile depends on the spatial coordinates x, y and z and the mode profile $|F(x,y)|^2$ because of gain saturation. However, in practice only a small portion of the fiber core is actually doped. If both the mode and dopant intensity are nearly uniform over the doped region, W can be assumed to be constant there and zero outside. Then Equation (3.59) can easily be integrated leading to;

$$g_0(z,t) = \Gamma_s \sigma_s W(z,t) \tag{3.61}$$

where Γ_s is the fraction of mode power within the doped region. Using Equation (3.61) and (3.51), the equation for gain dynamics can be found;

$$\frac{\partial g_0}{\partial t} = \frac{g_{ss} - g_0}{T_1} - \frac{g_0 |A|^2}{T_1 P_s^{sat}} \tag{3.62}$$

where $g_{ss} = \Gamma_s \sigma_s W_0$ is the small signal gain. For most fiber amplifiers the fluorescence time T_1 is long compared to the pulse width and hence spontaneous emission and pump power changes do not occur over the pulse duration, Equation (3.62) can be integrated, leading to;

$$g_0(z,t) \approx g_{ss} \exp\left(-\frac{1}{E_s}\int_{-\infty}^{t} |A(z,t')|^2 dt'\right) \tag{3.63}$$

where E_s is the saturation energy which is on the order of 1μJ for fiber amplifiers. This energy level is not reached in the lasers and fiber amplifiers, so gain saturation is negligible over the pulse duration. However, for a long pulse train, saturation can occur over timescales longer than T_1. The saturation is determined by the average power in the amplifier system $g_0 = g_{ss}(1 + P_{av}/P_s^{sat})^{-1}$.

Pulse propagation in an optical fiber is governed by a generalized NLSE (3.36) with coefficients β_1^{eff} and β_2^{eff} that are not only complex but also vary along the fiber length. In the specific case where the detuning parameter δ is zero, the NLSE can be written as;

$$\frac{\partial A}{\partial z} + \frac{i}{2}(\beta_2 + i g_0 T_2^2)\frac{\partial^2 A}{\partial T^2} = i\gamma(\omega_0)|A|^2 A + \frac{g_0 - \alpha}{2}A \tag{3.64}$$

where $T = t - \beta_1^{eff} z$ is the reduced time. The T_2 term accounts the decrease in gain for spectral components of the pulse far from the gain peak. This equation is called the "Master Equation of Mode-locking" [22].

3.3. Modelocking of Fiber Lasers

Mode-locking a laser leads to ultra-short pulses with duration of a few-ps or less. For this purpose a phase relation between the many longitudinal modes which can exist in a laser cavity should be found. In this section, the principle of only passive mode-locking will be introduced using an artificial saturable absorber, as this is the method implemented in the erbium-doped fiber laser used in this thesis.

An electromagnetic pulse propagating in a laser cavity can be denoted by a superposition of plane waves with different wavelengths. The possible wavelengths of the longitudinal modes are given by the condition;

$$n\lambda_n = 2L \tag{3.65}$$

where λ_n is the wavelength of the longitudinal mode and L is the cavity length. A large number of modes of different frequency can exist at the same time and each will be independent in phase and amplitude. Thus the total electric field in the cavity is given by the sum of the field of all modes;

$$E(z,t) = \sum_n E_n(z,t) = \sum_n E_{0,n}\, e^{ik_n z - i\omega_n t}, \qquad E_{0,n} = \left|E_{0,n}\right| e^{i\phi_n} \tag{3.66}$$

where $E_{0,n}$ is the complex amplitude of the n-th mode and ϕ_n its phase. Assuming equal amplitude for all modes, the intensity is;

$$I(z,t) \propto E(z,t)E^*(z,t) = |E_0|^2 \sum_{n=1}^{N} \sum_{m=1}^{N} e^{i(\phi_n - (\phi_m)(m-n)\Omega\left(\frac{z}{c} - t\right)} \tag{3.67}$$

where

$$\Omega = \omega_{n+1} - \omega_n = \frac{\pi c}{L} \tag{3.68}$$

being the frequency difference between two consecutive modes. If all modes have fixed phase relation, Equation (3.67) simplifies to;

$$I(z,t) \propto E(z,t)E^*(z,t) = |E_0|^2 e^{i\delta\phi} \sum_{n=1}^{N} \sum_{m=1}^{N} e^{i(m-n)\Omega\left(\frac{z}{c} - t\right)} \tag{3.69}$$

The second exponential part in the above equation will be 1 for all terms of the sum if the condition;

$$\Omega\left(\frac{z}{c} - t\right) = 2\pi j \quad \leftrightarrow \quad z - ct = 2Lj, \;\; j = 0,1,2,\ldots \tag{3.70}$$

holds. Then the maximum of Equation (3.69) is;

$$I_{max} = N^2|E_0|^2 \equiv N^2 I_0 \tag{3.71}$$

The temporal and spatial distances of neighboring pulses as a function of the intensity I_{max} can be derived from Equation (3.70) as;

$$\Delta z = 2L, \quad \Delta t = \frac{2L}{c} \equiv T \tag{3.72}$$

This means the intensity maxima repeat with the revolution time T of the laser resonator and there is one maximum inside the cavity at any time. Due to a fixed phase relation between the modes in the cavity, pulses with peak intensity I_{max} will grow, proportional to the square of the number of modes. To calculate the FWHM of the pulses, the superposition of N modes is assumed to be similar to the interference of N planar waves at a fixed time $t = 0$. Using geometric series;

$$I(t) = I_0 \frac{\sin^2\left(\frac{N\Omega}{2}t\right)}{\sin^2\left(\frac{\Omega}{2}t\right)} \tag{3.73}$$

The FWHM of the pulses can be derived from the above equation as;

$$I(\Delta T) = \frac{1}{2} I_{max} \quad \rightarrow \quad \Delta T = \frac{1}{N}\frac{2L}{c} = \frac{1}{N}T \tag{3.74}$$

The pulse width decreases with the number of superposed modes and is directly proportional to the revolution time of the laser cavity.

A phase relation between superposed modes can be achieved by a modulation of the gain of the cavity with the difference frequency Ω of subsequent modes. All techniques to get a mode-lock rely on this principle. Due to loss modulation, the electromagnetic field in the cavity gets additional time dependence;

$$E_n(z,t) = (E_{0,n} + E_n^{mod}\cos\Omega t)e^{ik_n z - i\omega_n t} \tag{3.75}$$

$$= \left[E_{0,n}e^{-i\omega_n t} + \frac{1}{2}E_n^{mod}(e^{-i\Omega t} + e^{i\Omega t})e^{-i\omega_n t}\right]e^{ik_n z}$$

$$= \left[E_{0,n}e^{-i\omega_n t} + \frac{1}{2}E_n^{mod}(e^{-i\omega_{n+1} t} + e^{-i\omega_{n-1} t})\right]e^{ik_n z}$$

The above equation hints that the time dependence induces sidebands in every mode whose frequencies coincide with the one of the neighboring modes. Since this is valid for the total bandwidth, a phase synchronization so called “mode-lock” between all longitudinal modes is achieved.

There are several ways to have mode-lock state in a laser. They are categorized by the method of how gain modulation is done. If an actively driven device, i.e. a switch or amplitude modulator is used, it will be active mode-locking, if a passive device like a saturable absorber is used, it will be passive mode-locking. However for the relevance of this thesis, only a special case of passive mode-locking will be explained in greater detail in the subsequent part.

In passive mode-locking the nonlinear component used to make mode-locked lasing more favorable than continuous-wave (cw) lasing simply introduces a higher loss at low power so that a short pulse with higher peak power experiences a stronger net gain.

Fiber lasers can also be mode-locked by using intensity dependent changes in the state of polarization when the orthogonally polarized components of a single pulse propagate inside an optical fiber. The polarization of the intense center of the pulse is rotated more than the less intense wings.

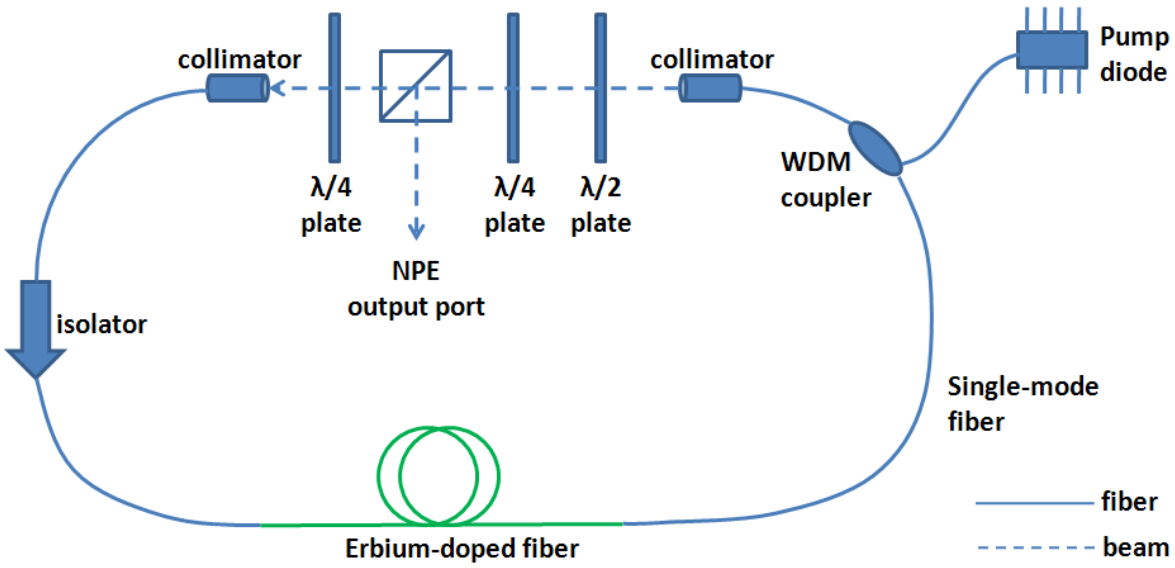

Figure 3.2. Schematic of a fiber ring laser mode-locked via NPE

The mode-locking process can be understood considering a fiber laser built in a ring configuration as shown in Figure 3.2. The pulse is linearly polarized after the polarizing beam splitter (PBS). The quarter wave plate following the PBS set the polarization to be

slightly elliptical, such that Kerr effect in the fiber section has a notable effect on the polarization of the pulse. After the fiber section, the polarization of the pulse center will differ from the polarization of the wings. The combination of quarter- and half-wave plate makes the polarization to be linear in the central part of the pulse, so the center of the pulse passes through the PBS cube and the wings are reflected out of the cavity through the nonlinear polarization evolution (NPE) port. The overall effect of the waveplates, PBS cube and fiber is shortening of the pulse after each round trip, with the PBS effectively acting as a saturable absorber.

The pulse at the beginning of the fiber section after free-space has to have elliptical polarization. The reason is explained as: The main contributors to the intensity dependence of the polarization evolution are self-phase and cross-phase modulation (SPM and XPM). Assuming the two eigenmodes are polarized along the x- and y-axis with intensity levels I_x and I_y, the total phase delays Φ_{x} and Φ_{y} along the axis can be obtained by adding the linear phase delays $\beta_x 2L$ and $\beta_y 2L$ as well as self- and cross-phase modulation term [23];

$$\Phi_{\mathrm{x}} = \left[\beta_x + \gamma I_x + \gamma \frac{2}{3} I_y\right] 2L \tag{3.76}$$

$$\Phi_{\mathrm{y}} = \left[\beta_y + \gamma I_y + \gamma \frac{2}{3} I_x\right] 2L \tag{3.77}$$

where L is the fiber length. The difference of the above equations gives the net phase shift between the two axes;

$$\Delta\Phi = \Phi_{\mathrm{x}} - \Phi_{\mathrm{y}} = \left[(\beta_x - \beta_y) + \gamma(I_x - I_y) + \gamma\frac{2}{3}(I_y - I_x)\right] 2L \tag{3.78}$$

Equation (3.78) suggests that circular input polarization does not lead to any intensity dependent phase shift, so the polarization of the pulse has to be elliptical when entering the fiber section of the cavity. This is achieved by the quarter-wave plate after the PBS cube.

Chapter 4

Laser Oscillator System and Characterization

Ultrafast fiber lasers have the potential to serve as master oscillators in accelerators. Pulse durations on the order of 100 fs are required to work in this area, hence the most promising candidate is a passively mode-locked laser through nonlinear polarization evolution. Noting these arguments, an erbium-doped fiber laser is selected to be used as the oscillator in this thesis for which components are widely available due to its operation at the telecommunication wavelength of 1550 nm.

4.1.Stretched-pulse vs. Stretched-spectrum Type Similaritons

One stability limit for mode-locking is the amount of nonlinear phase shift the pulse accumulates during one round trip. A soliton, the stable solution to the NLSE as discussed in Section 3.1, becomes unstable if it accumulates a phase shift of 2π or more per round trip. This would mean a soliton-laser's output power is limited to very small levels.

In an approach first found by Tamura *et.al*. in 1993 [24], alternating pieces of normal and anomalous dispersion fibers were combined to have breathing of the pulse duration one round trip, making the pulse short in the middle of the normal and anomalous pieces of the fiber cavity. This results in an effective decrease in peak power, as the pulse is only short

for a small portion of the fiber cavity. Since nonlinear effects are peak power dependent, the nonlinear phase shift accumulated per round trip is considerably decreased to the case of a soliton. In other words pulse energy that the laser can sustain before becoming unstable is increased, thus laser has a higher output power. A further increase in the output power can be achieved by construction a laser such that the net dispersion of the cavity is not zero but slightly positive. Therefore the pulse will not reach the transform limit inside the cavity and will always have a positive chirp. This will further increase the maximum energy of the pulse inside the cavity while still maintaining stability. However, compared to solitons, stretched-pulses require more pump power to achieve high enough peak power in order to have mode-locking sustained.

Pulse formation is dominated by a rich interplay between group velocity dispersion (GVD) and nonlinear effects [25-27]. Developments leading to better performance are typically triggered by new pulse shaping concepts and better understanding of underlying dynamics. Recent studies of Ilday *et. al.* showed experimental demonstration of a new laser type that can be regarded as a "stretched-spectrum" laser [28].

The establishment of self-similarity is a fundamental physical property that has been extensively studied to understand widely different nonlinear physical phenomena [29], including asymptotic self-similar behavior in radial pattern formation [30] and in stimulated Raman scattering [31], the evolution of self-written waveguides [32], and the formation of Cantor set fractals in soliton systems [33] in the field of nonlinear optics; the propagation of thermal waves in nuclear explosions, the formation of fractures in elastic solids, and the scaling properties of turbulent flow [34]. Kruglov *et. al.* [35] and Fermann *et.al.* [36] have developed self-similarity techniques that have recently been applied to

study pulse propagation in normal-dispersion fiber amplifiers, with the result showing that linearly chirped parabolic pulses are asymptotic self-similar solutions of the NLSE with a constant gain profile. These results have been confirmed experimentally and have extended previous theoretical and numerical studies of parabolic pulse propagation [37, 38]. Furthermore Ilday *et.al*. [39] have observed self-similar pulse evolution in a laser cavity. Recently Ilday *et. al.* reported first experimental and theoretical observation of stable pulses that propagate self-similarly in the presence of amplification (Kruglow-type) in a laser cavity [see [28] for details]. This corresponds to coexistence of dissipative self-similar solutions and soliton-like solutions to a modified NLSE subject to periodic boundary conditions. These solutions are robust enough against perturbations to be observed experimentally. A characteristic feature of Kruglow-type self-similar pulses is exponential broadening of the spectrum which must be undone at the end of each round trip. As such, periodic breathing of the spectrum is observed in the cavity due to alternate of interference filtering (bandwidth cutoff) and spectral-broadening in a single round trip.

4.2. Numerical Simulation of the Laser Oscillator

In this section, the numerical model used for simulating mode-locking of the erbium-doped fiber laser is presented. It is based on solving the NLSE (3.44) which was derived in chapter 3. The model includes the effects of saturable gain, second- and third-order dispersion, linear losses and nonlinear effects such as gain dispersion in the amplification section, self-phase modulation, Raman scattering, saturable absorption and bandpass filter. The pulse is assumed to start from noise and is iterated over many round trips until a steady state solution is reached. The simulator is based on a code written by Prof. F. Omer Ilday of

Bilkent University, and a Java interface written by Cagrı Senel, one of Ilday's students. It employs the split step Fourier method, which will be explained in the following subsection.

4.2.1. Split-step Fourier Method

A convenient way to solve the NLSE;

$$\frac{\partial A}{\partial z}+\frac{\alpha}{2}A+\frac{i\beta_2}{2}\frac{\partial^2 A}{\partial t^2}-\frac{\beta_3}{6}\frac{\partial^3 A}{\partial t^3}=i\gamma\left[|A|^2A+\frac{i}{\omega_0}\frac{\partial}{\partial T}(|A|^2A)-T_RA\frac{\partial|A|^2}{\partial T}\right] \quad (4.1)$$

is the split-step method. It assumes dispersion and nonlinear effects act independently over a short piece of fiber. It is practical to use Equation (4.1) as;

$$\frac{\partial A}{\partial z}=\left(\widehat{D}+\widehat{N}\right)A \quad (4.2)$$

where $\widehat{D}$ is the differential operator representing dispersion and absorption in a linear medium and $\widehat{N}$ is the nonlinear operator ruling all nonlinear effects on pulse propagation. These operators are given by;

$$\widehat{D}=-\frac{\alpha}{2}-\frac{i\beta_2}{2}\frac{\partial^2}{\partial t^2}+\frac{\beta_3}{6}\frac{\partial^3}{\partial t^3} \quad (4.3)$$

$$\widehat{N}=i\gamma\left[|A|^2+\frac{i}{\omega_0}\frac{1}{A}\frac{\partial}{\partial T}(|A|^2A)-T_R\frac{\partial|A|^2}{\partial T}\right] \quad (4.4)$$

The split-step Fourier method obtains an approximate solution by assuming that propagation over a small distance *h* is carried out in three steps. First, the pulse propagates over half the distance with only dispersive effects. Then, in the middle of the section, nonlinearity is included after which the pulse propagates again half the distance (Figure 4.1).

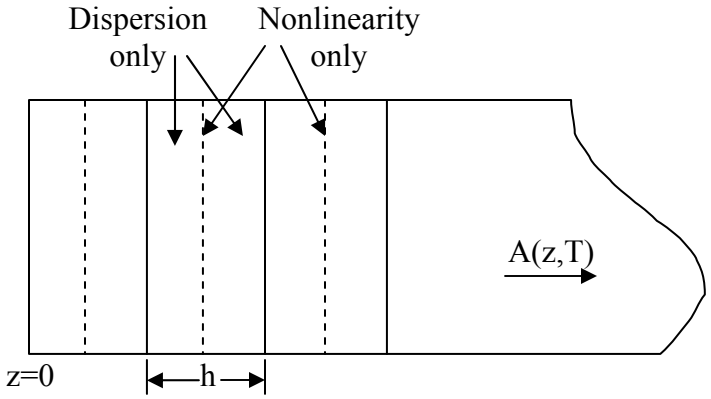

Figure 4.1. Illustration of split-step Fourier method used for numerical simulations

Mathematically,

$$A(z+h,T) \approx \exp\left(\frac{h}{2}\widehat{D}\right)\exp\left(\int_{z}^{z+h}\widehat{N}(z')dz'\right)\exp\left(\frac{h}{2}\widehat{D}\right)A(z,T) \tag{4.5}$$

The exponential operators can be evaluated in the Fourier domain. For the dispersive operator $\exp\left(\frac{h}{2}\widehat{D}\right)$, this yields

$$\exp\left(\frac{h}{2}\widehat{D}\right)A(z,T) = F_T^{-1}\exp\left(\frac{h}{2}\widehat{D}(i\omega)\right)F_T A(z,T) \tag{4.6}$$

where $F_T$denotes the fourier transform operation, $\hat{D}(i\omega)$ is obtained by replacing the differential operator $\partial/\partial T$ by $i\omega$. As $\hat{D}(i\omega)$ is just a number in the Fourier space, the evaluation of Equation (4.6) is straightforward (see [18] for details).

4.2.2. Simulator Interface

A screenshot of the simulator interface is shown in Figure 4.2. Table 4.1 summarizes the parameters needed for the numerics of the simulation.

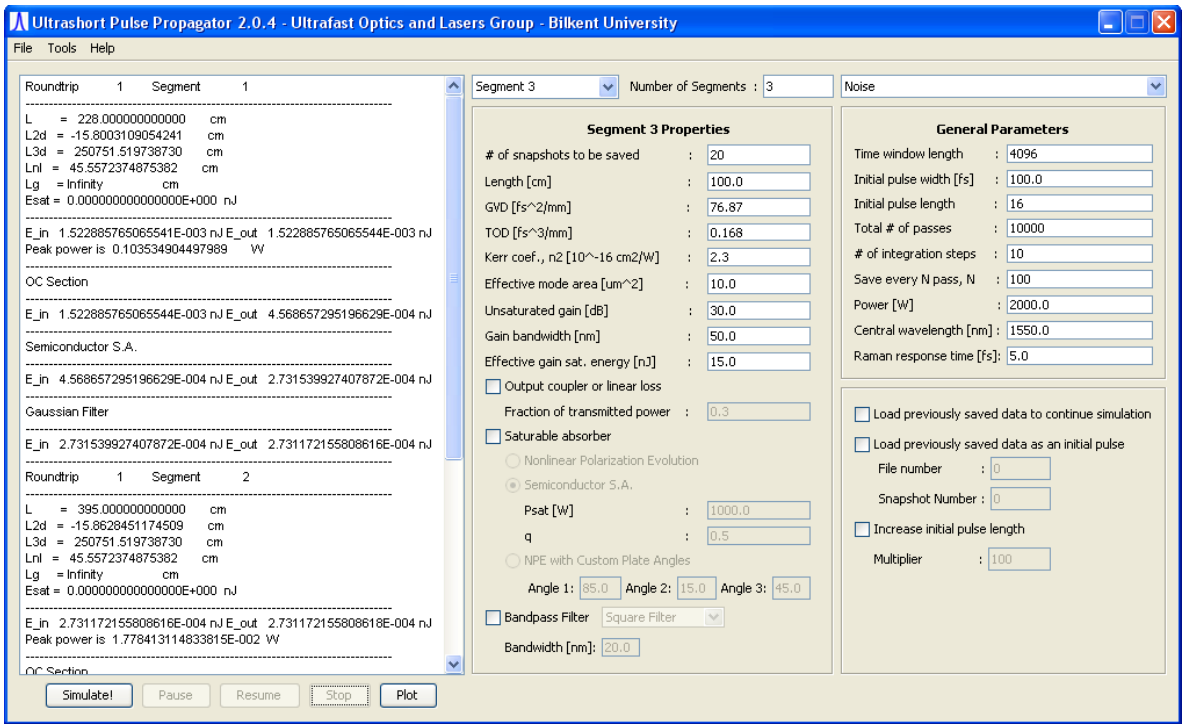

Figure 4.2. Screenshot of the simulator GUI

Parameter	***Function***
Time window length	Number of data points for discretizing time
Initial pulse width [fs]	Actual length of the pulse corresponding to a # of data points
Initial pulse length	# of discrete points representing the FWHM of initial pulse
Total # of passes	# of passes to be made over the entire sequence of segments
# of integration steps	# of discrete steps taken per each page per segment
Save every N pass, N	# of roundtrips after which data is saved to file
Power [W]	Actual power corresponding to unit size of power
Central wavelength [nm]	The central wavelength of the light used for simulation
Raman response time [fs]	Parameter characterizing the strength of the Raman effect
# of snapshots to be saved	# of segments each fiber section is divided into
Length [cm]	Physical length of the segment
GVD [fs^2/mm]	Second order dispersion parameter
TOD [fs^3/mm]	Third order dispersion parameter
Kerr coef., n_2 [10^{-16}cm2/W]	The Kerr nonlinearity coefficient
Effective mode area [μm^2]	Effective mode area for the propagating beam
Unsaturated gain [dB]	Small signal gain of the amplifier
Gain bandwidth [nm]	Finite gain bandwidth for parabolic approximation
Effective gain sat. energy	Saturation energy in arbitrary units for the gain
Output coupler/linear loss	Adds an output coupler to the end of the segment

Table 4.1. Numerical parameters needed for the simulator

The initial pulse shape can be one of the pre-defined pulse shapes ranging from Gaussian pulse shape to noise. Each segment of the laser should be configured separately. The saturable absorber is implemented at the end of a segment, by converting the total nonlinear phase shift accumulated over the round trip into an amplitude modulation. The semiconductor saturable absorber is modeled as;

$$I_{SSA} = 1 - \frac{q}{1 + {}^{I}/_{I_{sat}}} \tag{4.7}$$

where q is the modulation depth and $I_{sat}$is the saturation power of the saturable absorber. For nonlinear polarization evolution, the model is;

$$I_{NPESA} = (1 - q)\cos\left(\frac{\pi}{2}\frac{I}{I_{sat}}\right) \tag{4.8}$$

4.2.3. Simulation Results

Simulation of the laser is done with the parameters summarized in Table 4.2. A total of six segments are required for the actual imitation of the laser. However, number of segments severely increases processor usage. For practical purposes, laser is simulated after some approximations resulting in just three segments instead of six segments. This approximation and %5 uncertainty associated with fiber properties (mode-field diameter, core diameter, numerical aperture, etc.) caused minor mismatch in simulated and experimental results. The output coupler section of the simulation is approximated as the total loss due to %5 tap port at isolator in addition to the loss at the NPE output. Although NPE, output coupler and interference filter are separated by single mode fibers, they were

all assumed to be located at the end of first segment. Second- and third-order dispersion has been calculated from the data available in the component datasheets as dispersion depends linearly on core diameter and numerical aperture. There is no option for backward or forward pumping in the simulation, so any possible effect of backward pumping (experimental case) is not accounted for in the simulation results. Initial pulse is selected as noise for testing the simulation results. The numerical accuracy is also verified by checking that results are unaffected after doubling the sampling resolution.

Section	***Fiber type***	***Length (cm)***	***Dispersion (fs^2/cm)***	***Total dispersion (fs^2)***
Pump coupler	Lucent980	54.5	45.1	2457.95
polarizer	SMF28+PM Panda	33.5	-228.3	-7648.05
isolator	SMF28	40	-228.3	-9132
Collimator 1	SMF28	32.5	-228.3	-7419.75
Fiber Stretcher, collimator 2	SMF28	228.5	-228.3	-52166.55
Gain fiber	Lucent custom made Er-doped	100	768.7	76870
total				2961.6

Table 4.2. Length of fiber segments and dispersion properties for the laser

Figure 4.3 shows spectrum of the mode-locked laser which is a stable solution after 4500 roundtrips. In fact, laser can reach mode-lock state after around 50 roundtrips, but for the sake of stability check, pulse is rotated inside the cavity for 4500 roundtrips to achieve convergence to the last digit of the solution. Figure 4.4 shows buildup of the pulse from noise after 50 roundtrips.

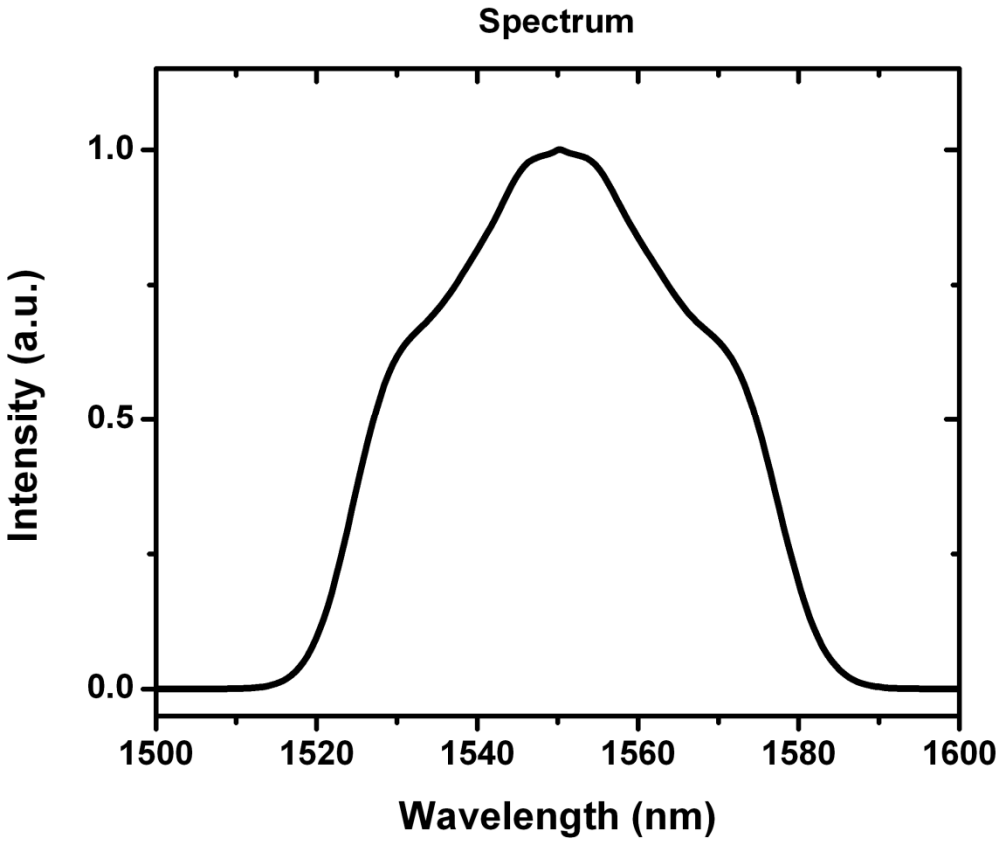

Figure 4.3. Simulated spectrum of the pulse

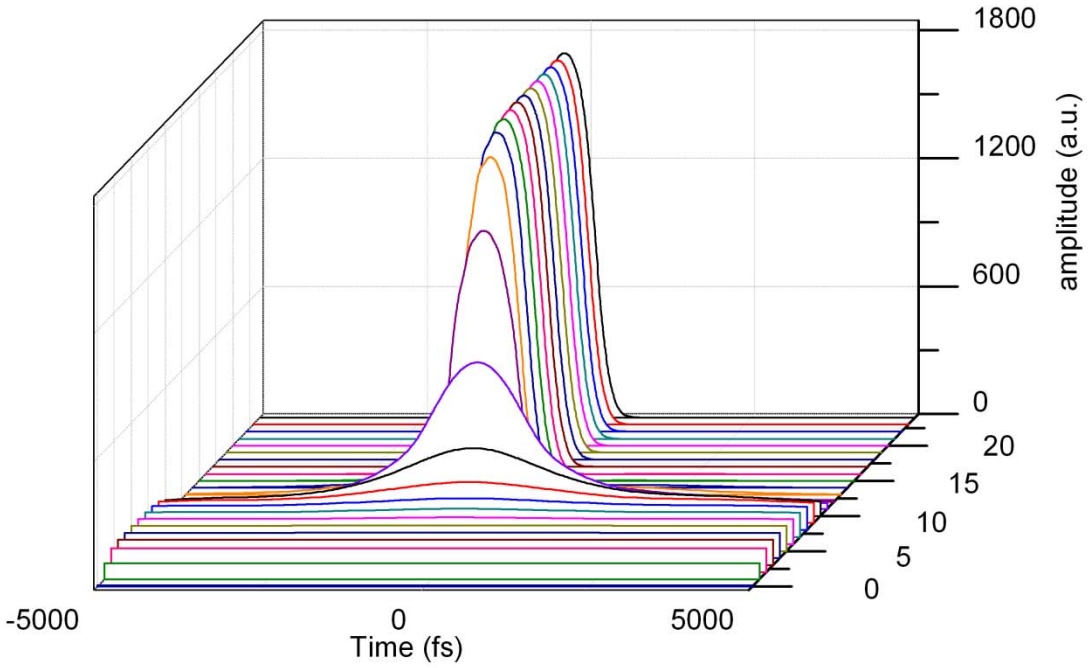

Figure 4.4. Buildup of the pulse inside the simulated cavity over 50 roundtrips

4.3. Setup of the Laser Oscillator

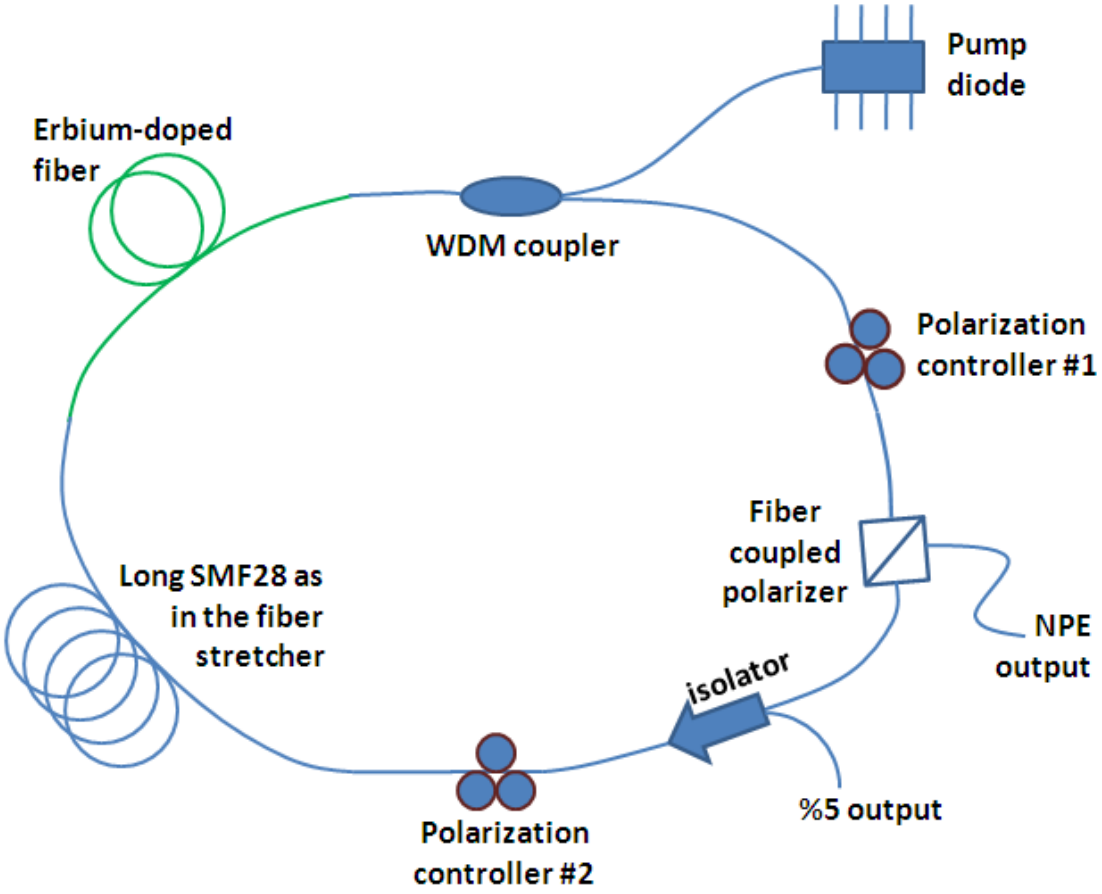

Figure 4.5. Schematic setup of the all-fiber stretched-pulse laser

Initially a stretched–pulse erbium-doped laser in all-fiber cavity configuration was constructed (Figure 4.5). It was very robust; however changing the repetition rate of an all-fiber laser is somewhat troublesome as it requires modifying the fiber lengths inside the cavity. Since the main goal of this thesis requires a laser oscillator of which the repetition rate is adjustable on the order of a few MHz, some modifications were made to the all-fiber

laser oscillator. Moreover, at that time an exciting-new discovery of a new laser type was found by Ilday *et.al.* of Bilkent University (see [28] for details). This new laser kind, regarded as "stretched-spectrum" laser was found to be very robust, even more so than the regular stretched-pulse laser. The difference between a stretched-spectrum and a stretched-pulse is that former one has an interference filter inside the cavity which inspires the name "stretched-spectrum" as spectral bandwidth of the pulse "breaths" through a round trip inside the cavity.

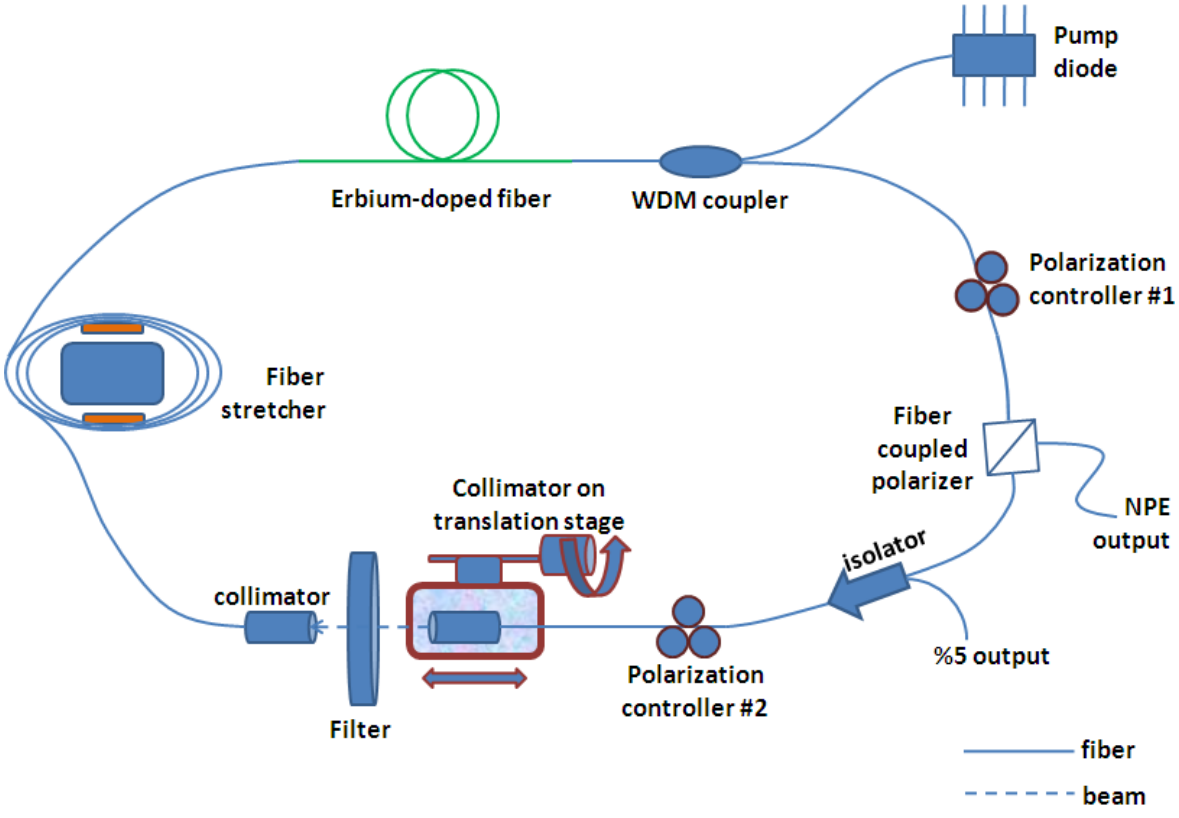

Figure 4.6. Schematic setup of the stretched-spectrum laser oscillator

As these two points taken into account, the latest laser design was finalized, which is depicted in Figure 4.6. Coherent with numerical simulations, an erbium-doped stretched-spectrum laser was constructed. The fiber section consists of 371.5 cm of regular single-mode fiber for 1550nm (SMF28), 17.5 cm of polarization maintaining fiber (PM panda) and 100 cm of highly doped (concentration of $6.10^{25}m^{-3}$) erbium fiber. Together with variable length free-space section, this gives a pulse repetition frequency of 40.6 MHz. Given the length of fibers the net GVD of the laser cavity was calculated to be about 2983 fs^2. Single mode fibers and polarization maintaining fiber has negative dispersion, and the gain fiber has positive dispersion. The laser is pumped by a single-mode laser diode with 300 mW power at 980 nm. The coupling to the cavity is done with a wavelength-division multiplexer (WDM). A WDM consists of two parallel fiber pieces, whose cores fused together by an electric arc. It is possible to obtain a wavelength dependent transmission from one fiber into the other, by adjusting the distance of the cores. If the transmission for one wavelength is 100% from fiber A to B, whereas the transmission from fiber B to A for another wavelength is zero; a WDM is obtained.

Since an upper harmonic of the laser's repetition rate needs to precisely match local oscillator's RF frequency (1.3 GHz), the free-space section has to be designed cautiously. Given that adjusting the repetition rate with fiber lengths is only an approximate and unpractical way, an adjustable free space section between two collimators has to be introduced. One of the collimators is mounted on a manual translation stage to coarsely adjust the repetition rate. However, the fine tuning is done with an in-line fiber stretcher which is an actuator for the phase-lock loop. The stretcher is located after the polarizer to avoid polarization distortions due to long fiber (~2.5 m) on it.

Apart from the fiber on the stretcher, most of the remaining fiber in the cavity is located on an aluminum plate which has a heater on its bottom to efficiently control the temperature of the fibers. Restraining the fiber temperature in smaller ranges than room conditions (with $0.1^{o}C$ sensitivity), actually gives better control over the stability of the laser. To further control the environment of the laser, a plexiglass box with 1 cm thickness is designed to fully encase it. This would ensure to minimize the susceptibility of the laser to external factors.

A detailed overview of the fiber lengths and dispersion coefficients is seen in Table 4.2 as the same parameters were also used as numerical simulation inputs. Two late photos of the laser oscillator is given in Figure 4.7.a and 4.7.b.

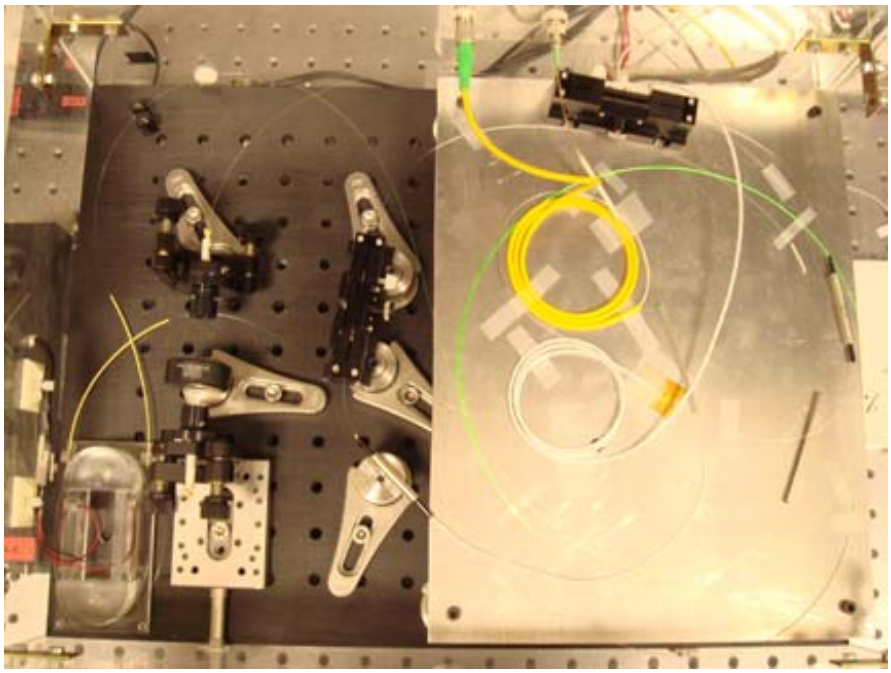

Figure 4.7.a. Photo of the laser cavity including the fiber stretcher and free-space section

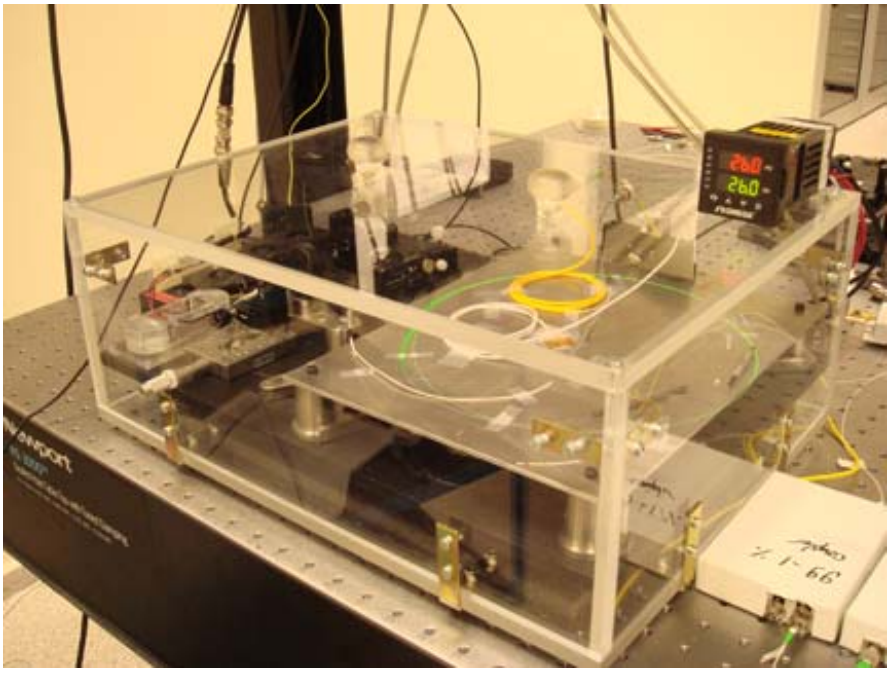

Figure 4.7.b. Photo of the fiber laser inside the custom-made box. Temperature controller is set to keep the temperature inside the box at 26^{o}C.

4.4. Pulse Characterization

Since the stabilization of the laser to an RF source only compensates phase fluctuations at low offset-frequencies, the phase-noise of the free-running laser has to be small in high offset-frequencies. Hence proper operation of the laser needs to be maintained. Autocorrelation, electric pulse train, optical and RF spectrum of the laser are monitored before stabilization of repetition rate.

4.4.1. Autocorrelation

Characterization of femtosecond laser pulses cannot be performed electronically since oscilloscopes and photo detectors do not have bandwidths on the order of a few hundred THz. For femtosecond pulses, autocorrelation technique has to be performed in the optical domain using nonlinear optical effects.

In this thesis intensity autocorrelation is used for temporal measurement of the pulse. Briefly, the technique depends on second-harmonic generation. Figure 4.8 illustrates the setup of autocorrelation. Initially the input pulse is split into two, and one of the pulses is delayed by τ. Then the two pulses are focused on a second-harmonic crystal in a non-collinear fashion. Assuming the material response is instantaneous, the convolution of two interfering signals or the induced nonlinear polarization simplifies to;

$$P^{(2)}(t) \propto E(t)E(t-\tau) \tag{4.9}$$

Since the photo detector's response is much longer than the pulse width, it integrates the incident light intensity leading to intensity autocorrelation;

$$I_{AC}(\tau) \propto \int_{-\infty}^{\infty} I(t)I(t-\tau)dt \tag{4.10}$$

with $I(t)$ being the intensity of the input pulse. Since the phase of the pulse is not conserved, Equation (4.10) does not contain full information about the pulse. However, if the pulse shape is known, the pulse width can be calculated by deconvolution of the correlation.

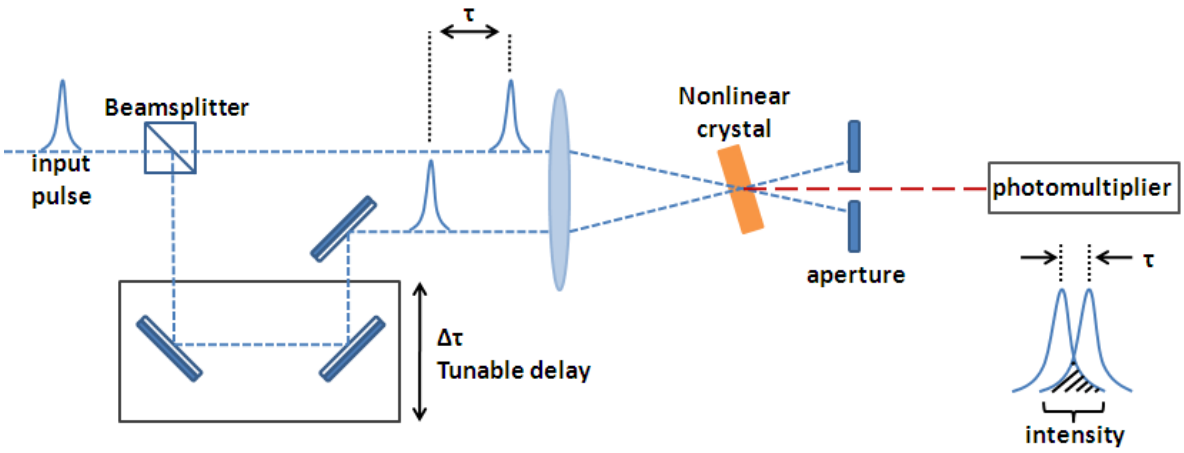

Figure 4.8.Setup of an intensity autocorrelation

Assuming a Gaussian pulse shape, a deconvolution factor of 0.707 is used in Equation 4.11, leading to 110 fs of pulse width (see Figure 4.9).

$$\Delta\tau_{Pulse}^{FWHM} = 0.707\Delta\tau_{Autocorrelation}^{FWHM} \tag{4.11}$$

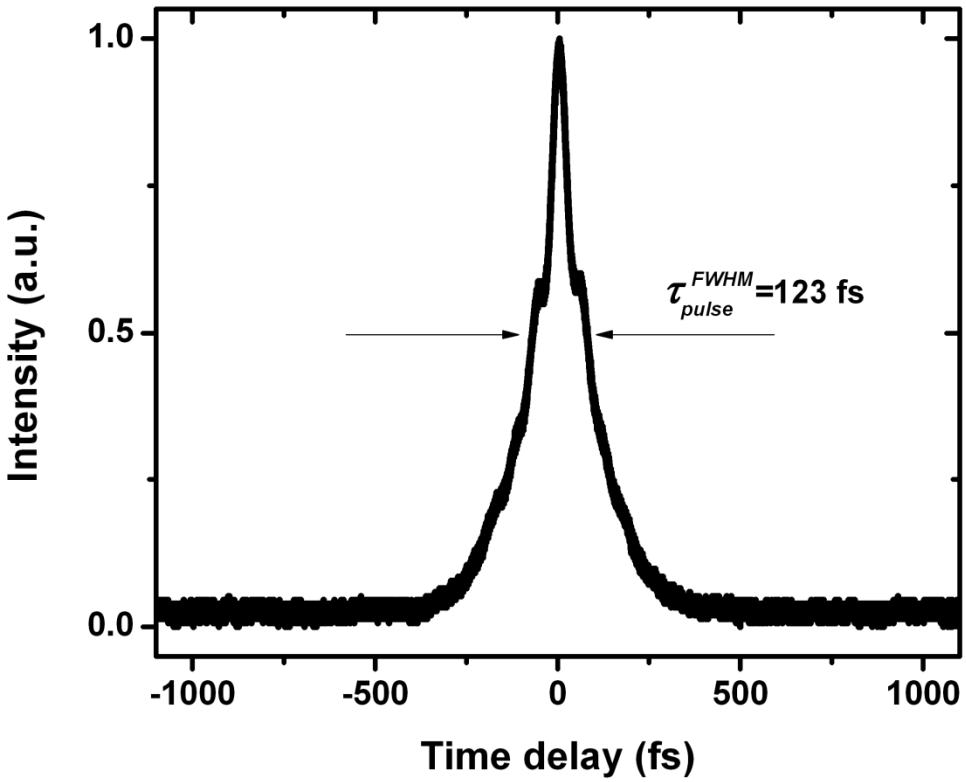

Figure 4.9. Autocorrelation of the laser pulse train

4.4.2. Optical & RF Spectrums and Pulse Train Measurements

If too much energy is accumulated inside the cavity, the laser will go into multiple-pulsing. To ensure proper operation of the laser, multiple-pulsing should be avoided. Optical spectrum together with RF spectrum and electrical pulse train on oscilloscope trace spans the whole bandwidth to check multiple-pulsing presence. Figures 4.10, 4.11 and 4.12 shows clear traces of these three measurements.

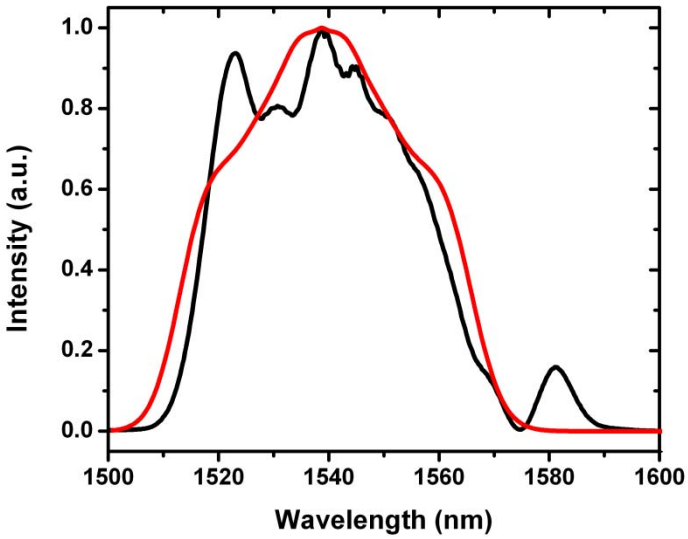

Figure 4.10. Measured optical spectrum of the pulse (simulation output – red)

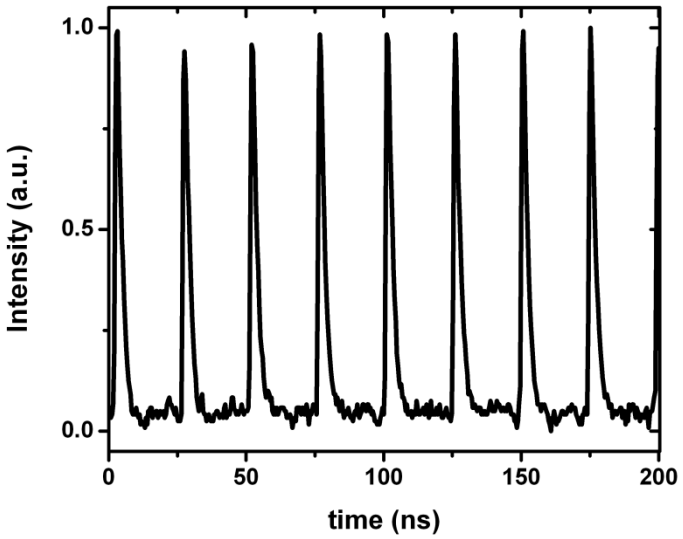

Figure 4.11. Oscilloscope trace of the laser with 40 MHz repetition rate

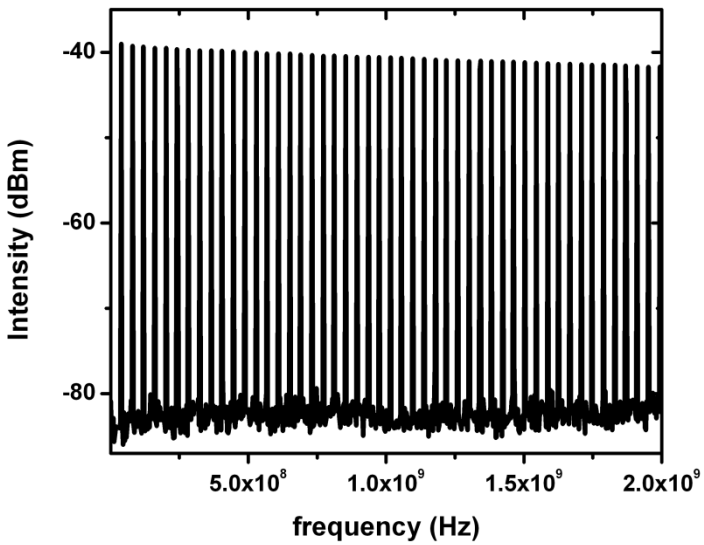

Figure 4.12. Photodiode response of the laser in frequency domain

Chapter 5

Phase Noise and Timing Jitter

5.1. Brief Introduction to Laser Phase Noise

A mode-locked laser produces train of pulses. The interval between consecutive pulses, defined as repetition period, is not identical for all neighboring pulses (Figure 5.1). The drift in pulse-to-pulse period is defined as the phase noise of the laser.

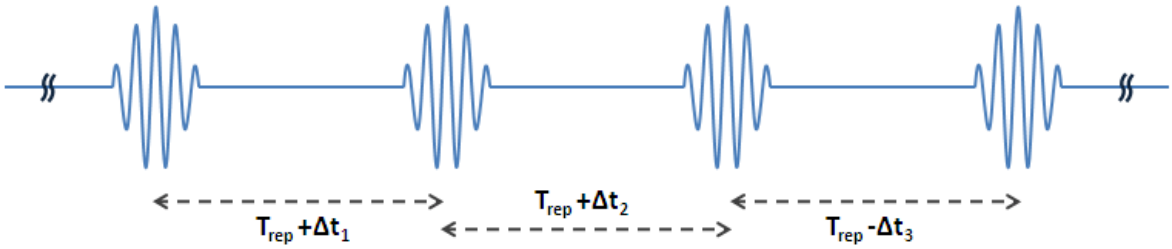

Figure 5.1. Time domain visualization of pulses from a mode-locked laser.

Although it is easier to picture phase noise in time domain, due to characteristics of test & measurement devices, phase noise is studied in frequency domain. To explain the frequency-domain response of phase noise, pulses need to be converted to frequency functions. To this end, applying a Fourier transform to time-domain pulses, gives a "frequency comb" (Figure 5.2).

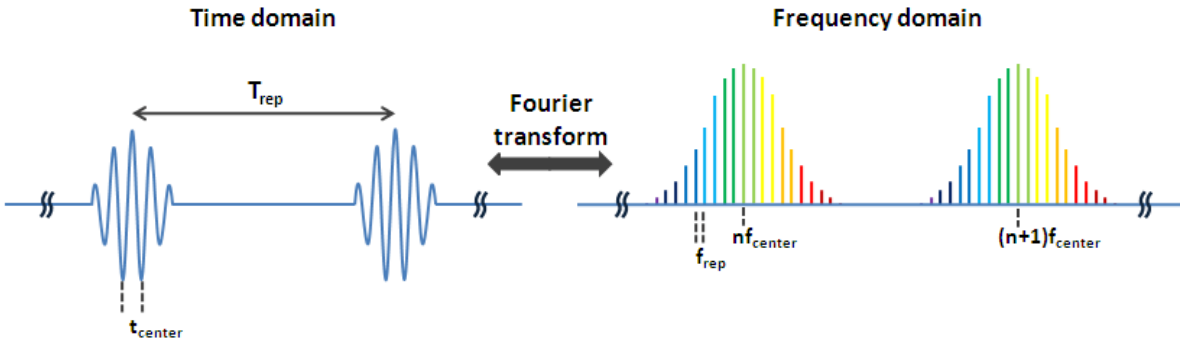

Figure 5.2. Time-to-frequency domain conversion of laser pulses.

In frequency domain phase noise or timing jitter corresponds to drift of individual comb lines. Ideally, comb lines are Dirac-delta functions. However, due to phase noise, actual comb lines have finite widths (Figure 5.3). The amount of this width is directly proportional to the timing jitter of a laser.

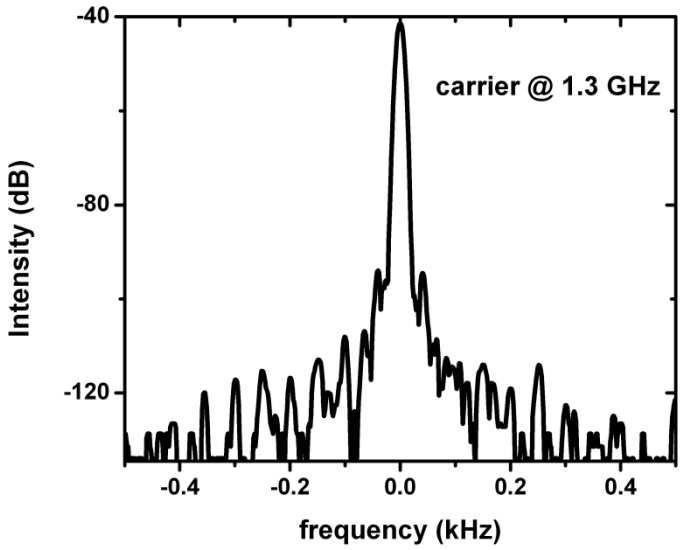

Figure 5.3. Single comb line of the laser at 1.3 GHz

5.2. Measuring Phase Noise of the Laser

Unlike the time picture, frequency response of the pulses covers THz bandwidth as well as much slower and measurable RF bandwidth. Frequency of a single comb line can be written as;

$$f = nf_{rep} + f_{ceo} \tag{5.1}$$

where n ranges from 0 to very large numbers on the order of 10^6, f_{rep} is the repetition rate of the laser and f_{ceo} is the offset frequency of carrier-envelope phase. f_{ceo} based studies are beyond the scope of this thesis and will not be mentioned in detail. Furthermore, converting the pulse into electrical signal via photodetection destroys the information about f_{ceo}, hence phase noise measurements covers only the timing jitter of repetition rate, f_{rep}. However it should be noted that ultimate stabilization of a pulsed laser also covers locking of f_{ceo} to an RF source.

Phase noise can be measured by selecting a single frequency comb line of the laser and phase locking it to a reference oscillator. To convert the pulses in electrical signals, a fast photodiode from EOT, ET3500 with 12 GHz bandwidth, is used. Unlike the Fourier picture, photodetection gives a comb line starting from DC (Figure 4.12).A single comb line (Figure 5.3) is selected by using a %1 bandwidth 1.3 GHz RF filter from Lorch Microwave (illustrated in Figure 5.4). After the filter, a low-noise amplifier from Mini-circuits, ZRL-1150LN+, is used; since the comb line needs to have above 0.1 mW power levels for measurement.

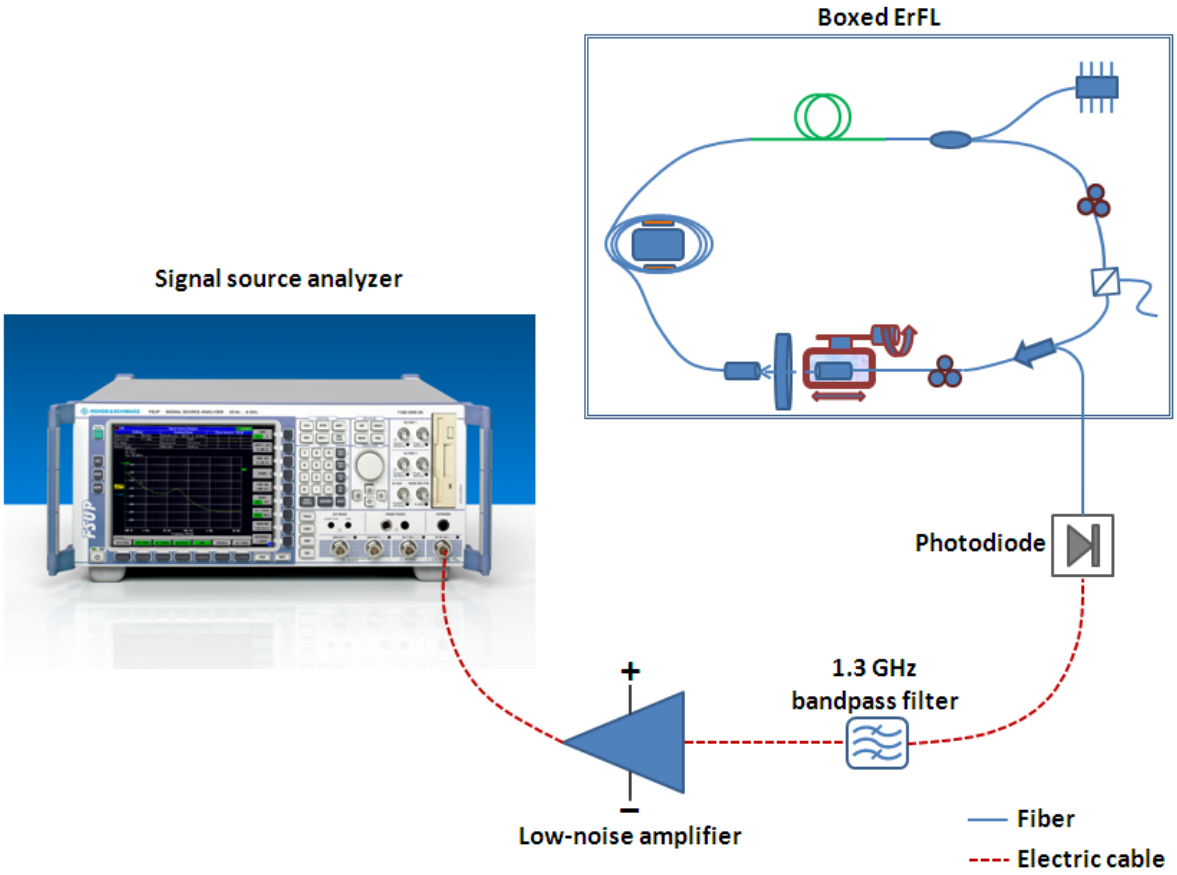

Figure 5.4. Phase noise measurement setup

A signal source analyzer (SSA) measures the phase noise of a signal by phase locking it to its local reference oscillator. A low-bandwidth phase-locked-loop (PLL) is required for this locking. Applying both the reference oscillator signal and DUT's (device under test) signal to a mixer and keeping a phase difference of $\pi/2$ between both signals (to suppress amplitude jitter) by the PLL, makes the mixer output signal zero. The remaining fluctuations represent the timing jitter between the two signals. This output is then sampled

by an A/D conversion system with high dynamic range and finally signal processing (FFT) gives the phase noise of the test signal as a function of frequency (Figure 5.5).

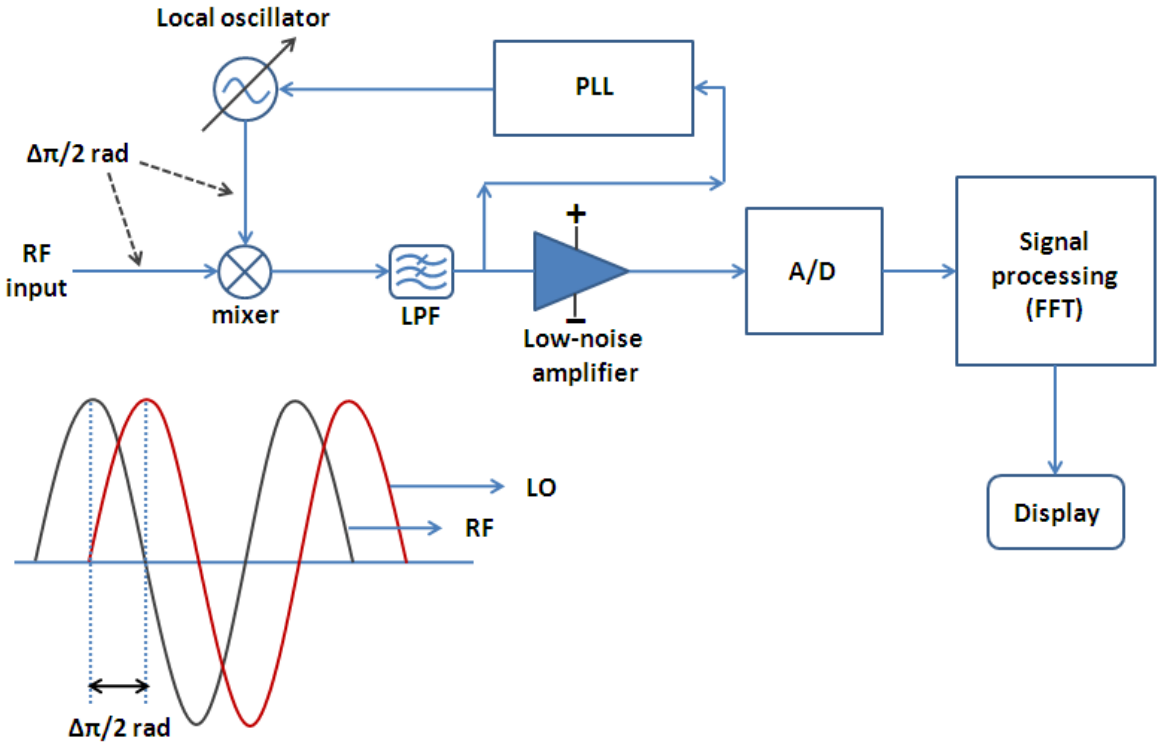

Figure 5.5. Schematic of a phase noise measurement using SSA (from [40])

Mathematically, when the test signal is phase locked to the internal reference, both signals are in quadrature or have $\pi/2$ phase difference. Assume;

$$V_{LO}(t) = A_{LO}\sin(\omega_c t + \Delta\phi_{LO}) \quad \text{and} \quad V_{DUT}(t) = A_{DUT}\cos(\omega_c t + \Delta\phi_{DUT}) \tag{5.2}$$

where ω_c is the common frequency for both signals, A_{LO}, A_{DUT} are amplitudes and $\Delta\phi_{LO}$, $\Delta\phi_{DUT}$ are phase jitter of either signal. The (ideal) frequency mixer multiplies the two signals which yields;

$$V_{mixer} = V_{LO}(t)V_{DUT}(t) = A_{LO}A_{DUT}\sin(\omega_c t + \Delta\phi_{LO})\cos(\omega_c t + \Delta\phi_{DUT})$$

$$= \frac{1}{2}A_{LO}A_{DUT}[\sin(2\omega_c t + \Delta\phi_{LO} + \Delta\phi_{DUT}) + \sin(\Delta\phi_{LO} - \Delta\phi_{DUT})] \tag{5.3}$$

using the trigonometric identity, $\sin(a \pm b) = \sin(a)\cos(b) \pm \cos(a)\sin(b)$. The low pass filter after the mixer eliminates the sum frequency, which results;

$$V_{filtered} = \frac{1}{2}A_{LO}A_{DUT}\sin(\Delta\phi_{LO} - \Delta\phi_{DUT}) \tag{5.4}$$

Since the phase fluctuations are small, low pass filter output can be approximated using $\sin(\Delta\phi_{LO} - \Delta\phi_{DUT}) \approx \Delta\phi_{LO} - \Delta\phi_{DUT}$. So the phase fluctuation between the local reference oscillator and the test signal is measured. However, this technique has a basic requirement; the phase noise of the local oscillator has to be small compared to the phase noise of the test signal.

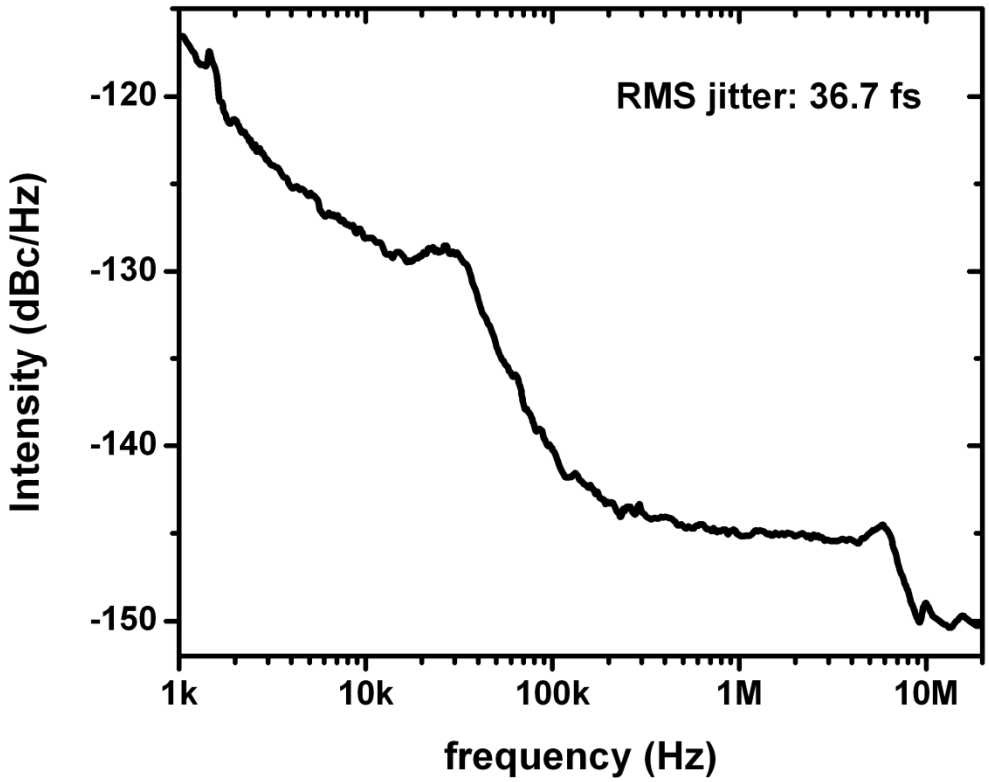

Figure 5.6. Single sideband phase noise for the laser oscillator in free-running mode.

Figure 5.6 shows a phase noise measurement of the free-running laser at 1.3 GHz from 1 kHz (due to upper state lifetime of erbium) to the Nyquist frequency, 20 MHz. A calculated RMS timing jitter of 36.7 fs is found from Equation (5.5) (see [41] for the details);

$$J_{RMS}|_{f_1}^{f_2} = \frac{1}{2\pi f_c}\sqrt{\int_{f_1}^{f_2} 2.10^{\frac{L(f)}{10}} df} \tag{5.5}$$

where f_c is the carrier frequency under test and $L(f)$ is the noise density in dBc/Hz unit.

Chapter 6

Synchronization Circuit and Experimental Results

6.1. Laser Synchronization

Thanks to the manual translation stage inside the cavity, laser has a variable repetition rate of 40.6 MHz within 1 MHz range. The 32^{th} harmonic of the laser repetition rate is at the studied synchronization frequency of 1.3 GHz. The laser is synchronized to a dielectric resonator oscillator (DRO) from Poseidon Scientific Instruments (PSI) using a phase-locked loop (PLL). Generated error signal by comparing the 32^{th} harmonic of the laser to the DRO is fed back to a fiber stretcher inside the laser cavity. Hence the fiber length of the cavity is controlled and the repetition rate is adjusted with respect to the reference oscillator.

The error signal is generated through a PLL circuit. After converting the laser output to electrical signal via photodetection, only 32^{th} harmonic of the repetition rate is selected by a bandpass filter. Following the filter the single harmonic is 30 dB amplified by a low-noise RF amplifier to have enough power at the mixer input. The frequency mixer multiplies the amplified optic-to-RF converted laser harmonic and the DRO output generating both the sum and difference frequencies of both sources. A low-pass filter is connected to the output port of the mixer to eliminate the sum frequency. The filtered signal is then feed to a

control loop feedback mechanism which is a proportional-integral-derivative controller (PID controller). The corrective signal generated in the PID controller is then amplified with a power amplifier to drive the high-capacitive piezoelectric fiber stretcher inside the laser cavity, onto which 2 meters of laser fiber are wound. Finally, the fiber wound on the piezo wafers stretches and compresses to modify the repetition rate of the laser in accordance with the corrective signal. A schematic overview and a photographed operation of the system is given in Figure 6.1 and 6.2 respectively.

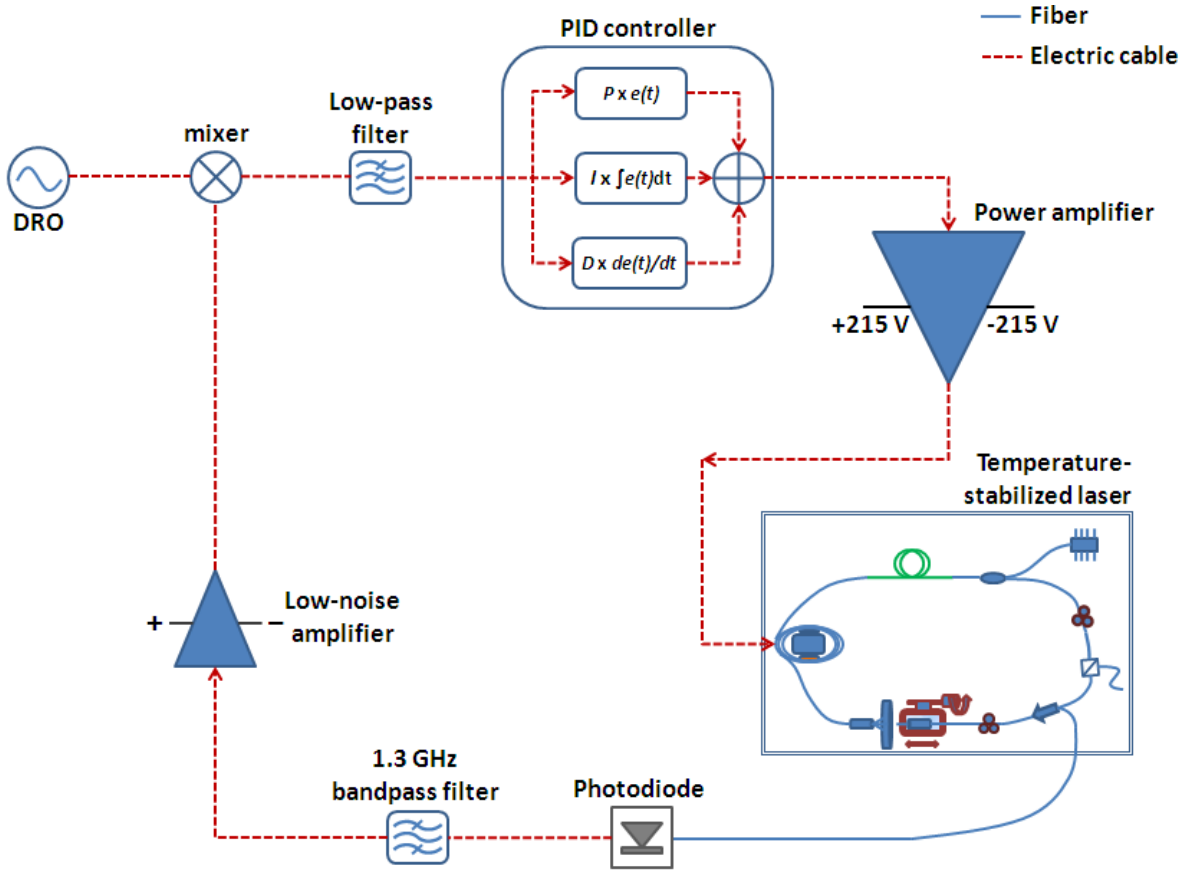

Figure 6.1. Schematic setup of the PLL system

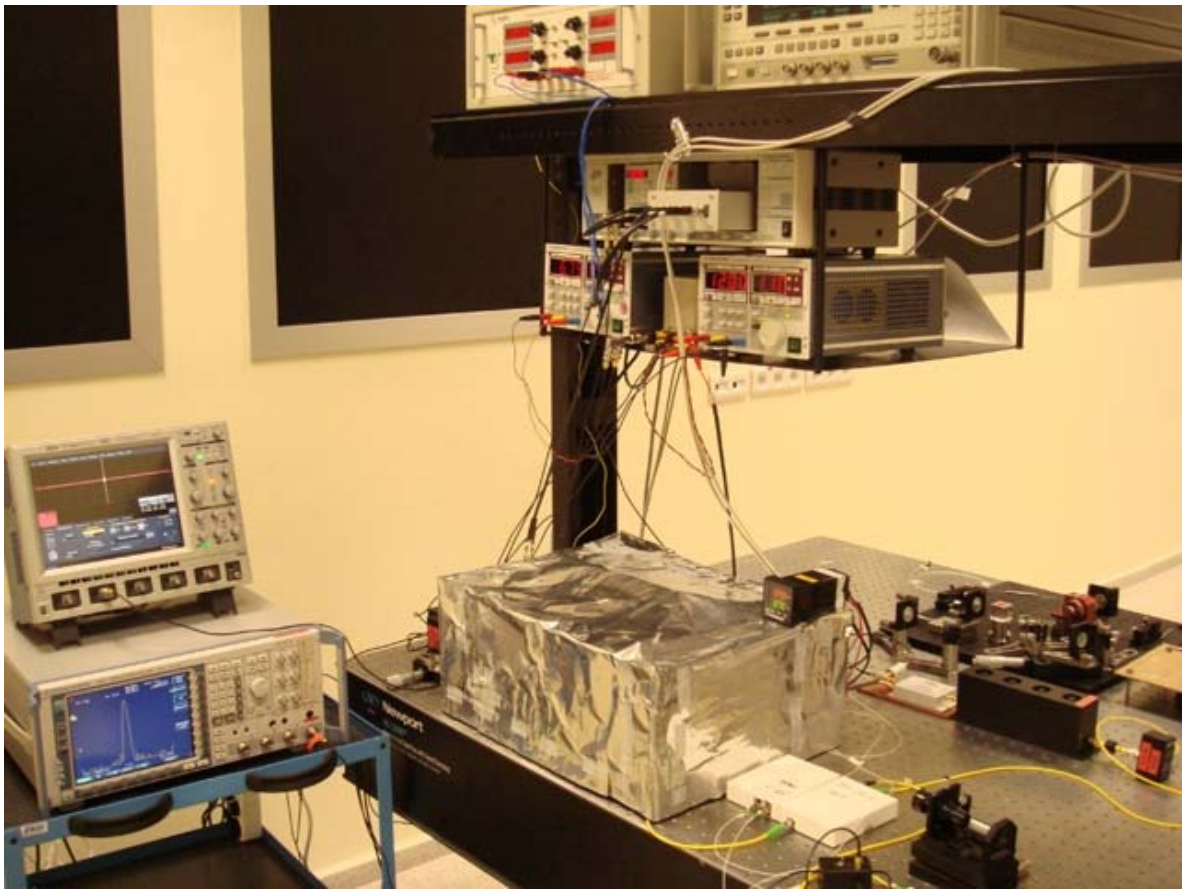

Figure 6.2. Photograph of the system in operation. Error signal is monitored on the oscilloscope screen and the harmonic of the laser is monitored on the RF spectrum analyzer. Laser box is covered with thin metal sheet for temperature isolation.

6.1.1. Fundamental Components of the Electronic System

Apart from the laser oscillator, the PLL system consists of various electronic components. Namely low-noise RF amplifier, power amplifier, band-pass and low-pass filters, frequency mixer, PID controller, DRO, photodetector and piezoelectric fiber stretcher are the components in the PLL. Except the power amplifier, remaining components are retail products.

Most of the RF components; low-noise amplifier (ZRL-1150LN+), low-pass filter(SLP-1.9+) and frequency mixer (ZX05-5+) are from Mini-circuits. Low-noise amplifier has a gain bandwidth of 750 MHz ranging from 650 to 1400 MHz. 30 dB typical gain is provided by 12 V dc supply. The ratio of output noise to that which would remain if the amplifier itself did not introduce noise, in other words noise figure is 1.1 dB. Low-pass filter has a passband of DC to 1.9 MHz. Stopband extends up to 400 MHz with loss more than 40 dB, hence attenuating the sum frequency after the mixer at least ten thousand times. Below 100 kHz, its insertion loss is 0.09 dB. The frequency mixer operates between 5-1500 MHz with typical input powers of 7 dBm. (see [42] for details)

Band-pass filter (4CF2-1300/13-S) is a product of Lorch-microwave. It has center frequency at 1.3 GHz, Q-factor of 2.9 and a 3 dB bandwidth of %1 corresponding to 13 MHz. (see [43] for details).

PID controller (SIM960) is on the product line of Stanford Research Systems. It has a bandwidth of 100 kHz with low-noise performance ($8\text{nV}/\sqrt{\text{hz}}$ above 10 Hz). The PID controller attempts to correct the error signal between the DRO and the laser harmonic by calculating and outputting a corrective signal back to the PLL. By adjusting the three gain

parameters of the PID controller, sufficient output to keep the loop in phase is generated. The proportional gain determines the reaction to the current error, the integral gain determines the reaction to the sum of recent errors and the derivative gain determines the reaction to the rate of change in the error. Mathematically, the PID controller calculates the formula;

$$\varepsilon = setpoint - measure \tag{6.1}$$

$$Output = P \times \left\{ \varepsilon + I \int \varepsilon dt + D \frac{d\varepsilon}{dt} \right\} + offset \tag{6.2}$$

where ε is the error signal, $setpoint$ is the reference signal and $measure$ is the processed signal (laser harmonic).

Power amplifier is designed and built by Dr. Aykutlu Dana of Bilkent University. PA85 from Apex Microtechnology is used as high-voltage, inverting power operational amplifier in the design. The power amplifier has a gain of 13 dB and supports output voltages between -210 to +210 V DC with ±215 V DC supply. V_{out}/V_{in} graph is given in Figure 6.3.

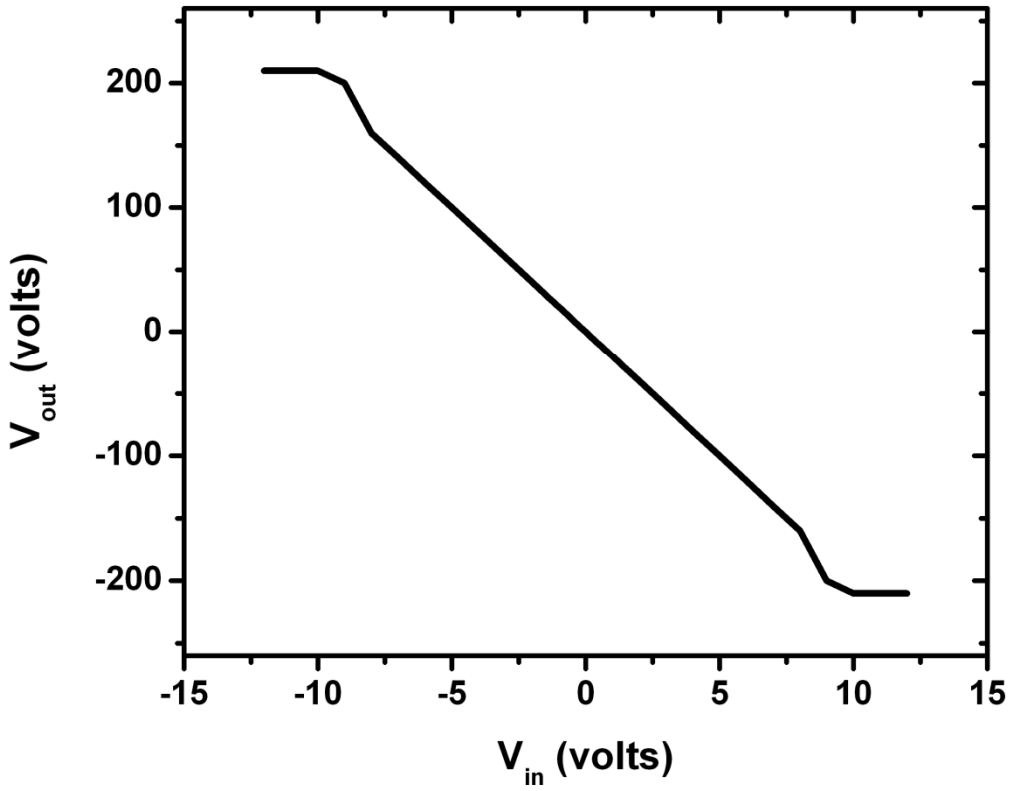

Figure 6.3. Gain response of the power amplifier. Saturation after ±10 V DC input voltage with ±215 V DC supply.

An ultra-low noise dielectric resonator oscillator from Poseidon Scientific Instruments is used as the reference signal source (DRO-1.300-FR). It has a center frequency of 1.3 GHz with ±100 ppm mechanical tuning range. It also has the option to control the center frequency by voltage controller oscillator (VCO) input, featuring 3 ppm/Volt typical control rate within ±10 V VCO input range. Typical phase noise performance of the DRO measured by the company is given in Table 6.1. (see [44] for details)

Carrier offset frequency	***Guaranteed phase noise***	***Typical phase noise***
@100 Hz	-87 dBc/Hz	-89 dBc/Hz
@1 kHz	-117 dBc/Hz	-119 dBc/Hz
@10 kHz	-140 dBc/Hz	-147 dBc/Hz
@100 kHz	-165 dBc/Hz	-169 dBc/Hz
@1 MHz	-170 dBc/Hz	< -175 dBc/Hz
@ 6 MHz	-170 dBc/Hz	< -175 dBc/Hz

However, these noise levels are lower than the given phase noise measurements of the DRO in the actual setup in the following section due to the fact than measurement instruments are different and more importantly, the company measured the noise of two DROs with 3dB subtracted at the end.

A fast photodetector from Electro-optics Technology is used for the electro-optic conversion of the laser pulses (ET-3500F). Covering the spectral range of 1000-1650 nm, this InGaAs photodetector has a bandwidth of 12 GHz and rise-, fall-times of <35ps. Noise equivalent power of the detector is below 0.04 $pV/\sqrt{hz}$. (see [45] for details)

Piezoelectric fiber stretcher is produced by Canadian Instrumentation and Research. Ltd. It compresses/stretches the fiber by applied voltage to piezo wafers onto which 5 rounds of fiber is wounded (approximately 200 cm of fiber). It has a bandwidth of 100 kHz and an applied voltage limitation of ±200 V DC to the piezo wafers. Within this voltage limitation, it can handle maximum repetition rate change of ±93 Hz which corresponds to a range of ±3 kHz around the center frequency at 1.3 GHz corresponding harmonic.

6.1.2. Performance Analysis of the PLL

The PLL is optimized such that the frequency range in which the laser and the DRO stay in phase is maximized. Without losing the lock, DRO frequency can be changed in the range of ±3 kHz via the VCO input. This is achieved by setting the PID controller gain parameters as -32 proportional gain, 5 integration gain and $0.2\text{x}10^{-5}$ differential gain. The range can be further increased by increasing the gain parameters in the PID controller, however increasing the gain causes the corrective signal to exceed the saturation point of the power amplifier (Figure 6.3), hence causing the locked error signal to have modulation and after a point destroys the lock.

When the PLL is not in operation, the laser harmonic and the reference DRO signal are not phase locked. Mathematically, additional terms will be added to the arguments of sinusoidal functions in Equation (5.2) which are ϕ_{LO} and ϕ_{DUT}, constant phases of the DRO and the laser harmonic respectively. Taking into account these new terms will also result in modifying Equation (5.4) as;

$$V_{filtered} = \frac{1}{2} A_{LO} A_{DUT} \sin(\phi_{LO} - \phi_{LO} + \Delta\phi_{LO} - \Delta\phi_{DUT}) \tag{6.3}$$

Hence the approximation made in Section 5.2 for phase noise measurement is not valid anymore. This unlocked error signal is monitored on the oscilloscope trace as sinusoidal wave. However when the system is in lock the two signals will be in phase ($\phi_{LO} = \phi_{DUT}$) and Equation 6.3 can be approximated as $\sin(\Delta\phi_{LO} - \Delta\phi_{DUT}) \approx \Delta\phi_{LO} - \Delta\phi_{DUT}$ generating a DC signal instead of a sinusoidal one.

The performance of the PLL was measured recording this DC signal over 41.3 hours. Although the system was observed to stay in lock for much longer times (possibly indefinitely) in absence of intentional halts or excessive distortion, memory limitations force the recording time to be relatively small. 41.3 hours of recording is given in Figure 6.4. Because of the memory limitation, the whole data points were not plotted. Instead rms of 100 seconds data chunks are given, which actually indicates if the lock was distorted or not. Figure 6.4 also includes rms error signal for the case where the lock is interrupted.

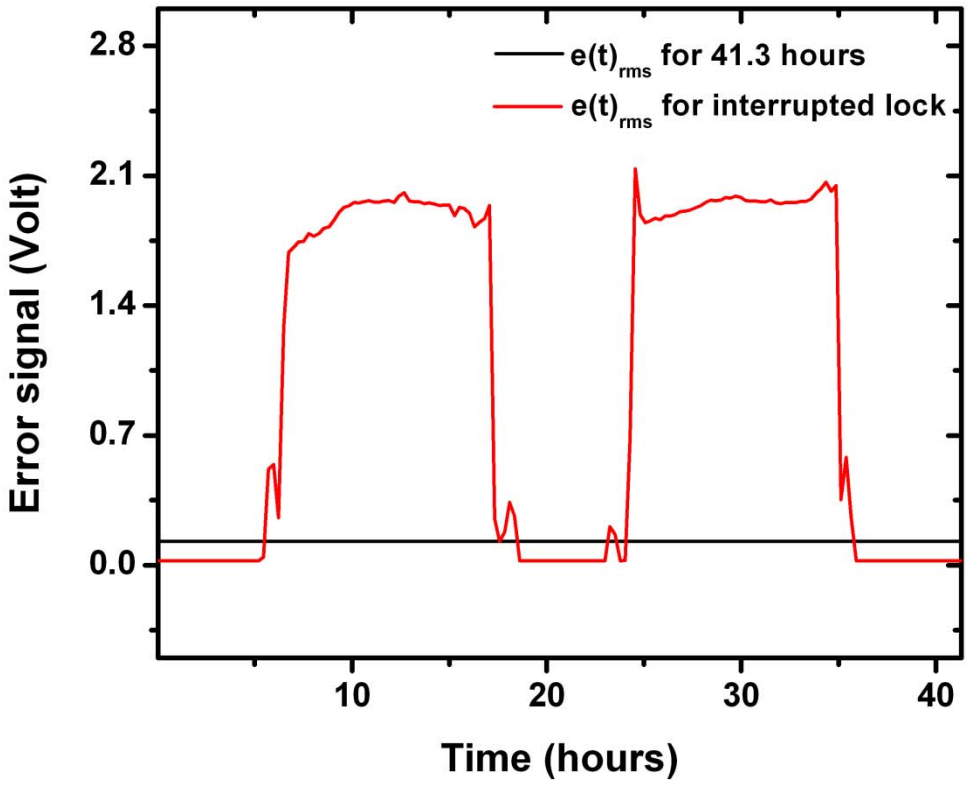

Figure 6.4. Performance record of the PLL (black line). Distorted lock (red line).

6.2. Synchronization Results in Phase Noise

Comparing the phase noise performance of the free-running laser and the DRO, it is shown that at high frequencies (1 kHz to 20 MHz, Nyquist frequency of the laser) the laser is only 1.5 times worse in stability than the DRO and it even outperforms the DRO up to 5kHz offset frequencies (Figure 6.5).

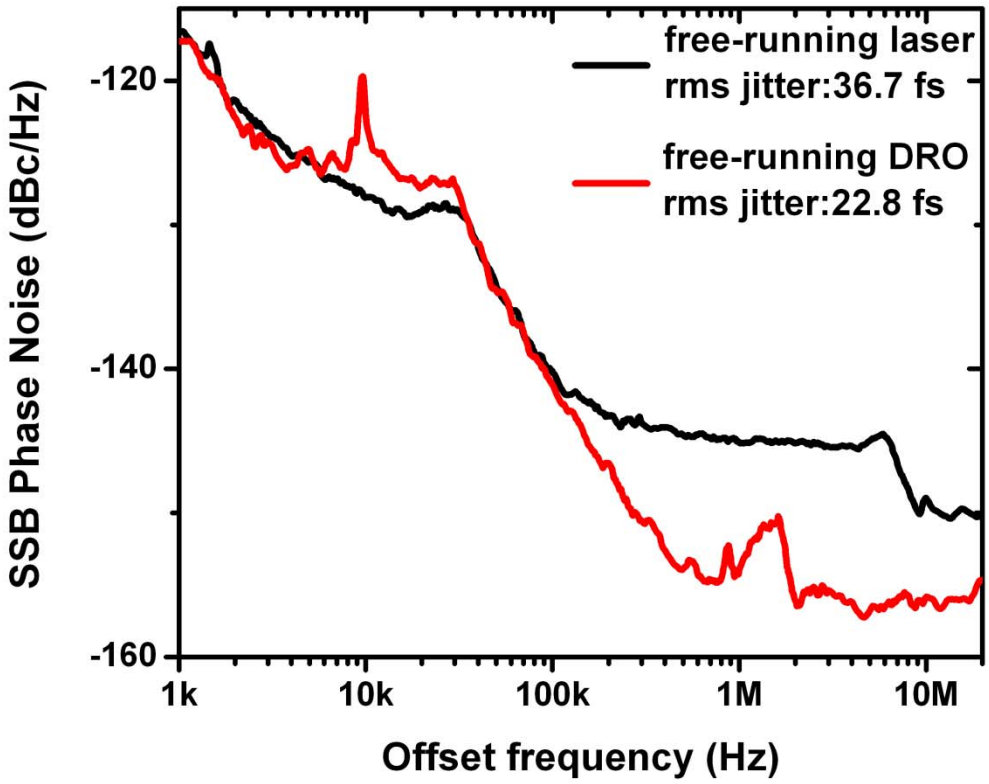

Figure 6.5. Free-running laser and DRO phase noise comparison

However, having less phase noise in laser up to 5 kHz range avoids noticing the effect of the stabilization in terms of phase noise improvement since the bandwidth of the PLL is 100 kHz. Therefore, one can either decrease the phase noise of the DRO or intentionally increase the phase noise of the laser at low frequencies. Since the DRO in use is not a low-noise crystal reference phase-locked DRO, the latter option would be exercised. As the laser oscillator is encased, external disturbances are decreased to minimum which further decreases its phase noise. Even removing the casing does not increase laser's phase noise above DRO's phase noise, so additional disturbance is created by literally having the laser to listen to random songs. The effect is given on Figure 6.6. Substantial phase noise is added to the laser at low frequencies (below 1 kHz). Figure 6.6 also depicts that above 100 kHz offset frequencies, the free-running DRO has the lowest phase noise which certainly would not be transmitted to the laser when they are in lock because of the limitation in PLL bandwidth (100 kHz). Yet, the laser has excellent stability at these frequencies.

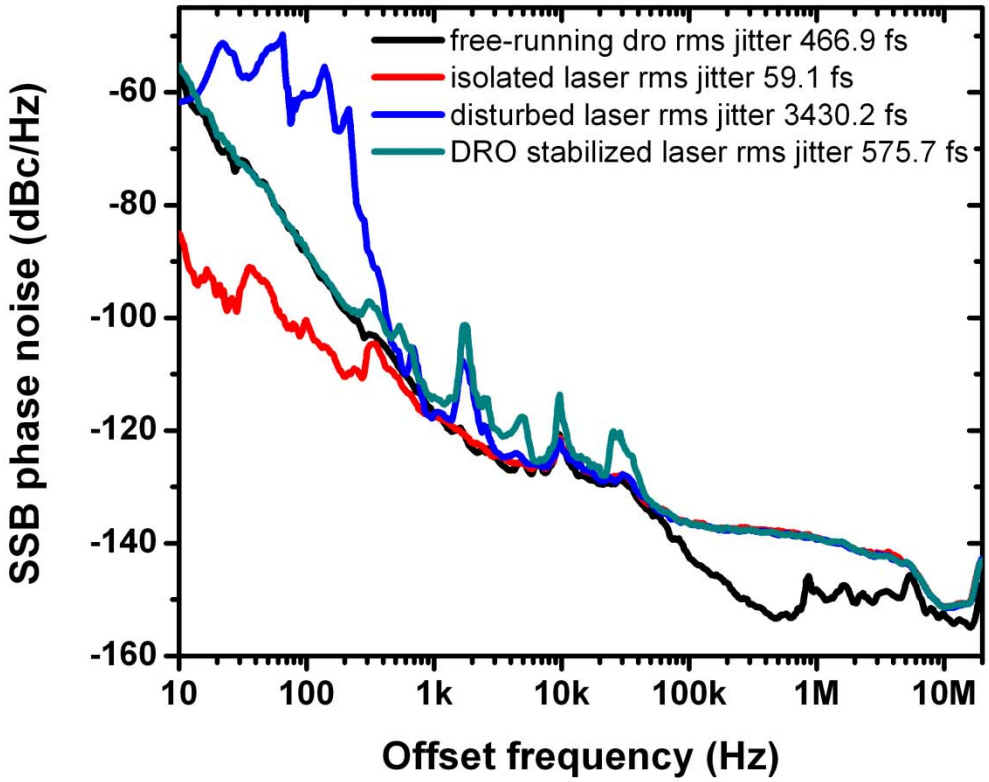

Figure 6.6. Phase noise comparison of the DRO and the laser at various conditions.

Figure 6.7 magnifies the section of Figure 6.6 where actual effect of locking loop is seen. Comparing the rms jitter stored only in this region, PLL actually improves the stability of the disturbed laser to the level of the DRO.

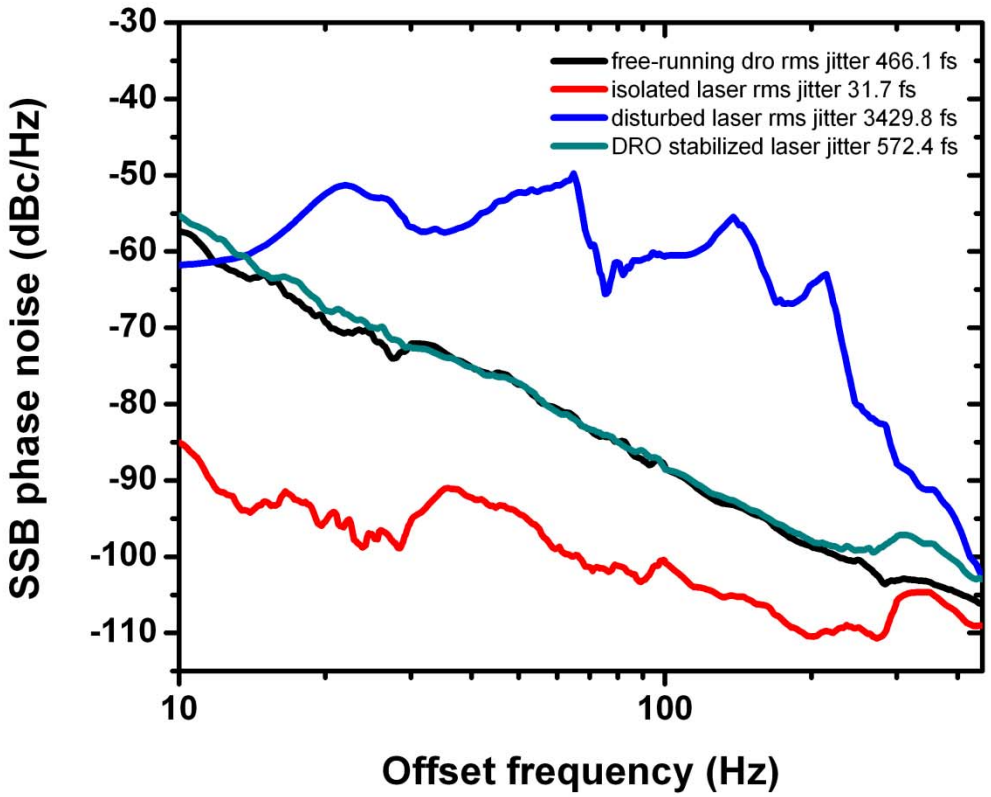

Figure 6.7. Zoomed in section of the phase noise graph to show the PLL effect on the laser's stability.

Chapter 7

Conclusion and Outlook

Based on the frequency response of ultrafast laser pulses, a fiber laser's repetition-rate stabilization system has been built and studied in this thesis.

Due to its excellent stability and robustness, a stretched-spectrum fiber laser was developed to serve as the core of the system producing optical pulses of 123 fs in transform limit. In agreement with numerical simulations, experimental construction of the laser oscillator had been pursued to the point of utmost completion. A manually adjustable free-space length was introduced to have the ability to shift the repetition rate in small amounts such that the upper harmonic frequency used for the PLL is roughly adjusted. For fine adjustment a piezoelectric fiber stretcher was integrated inside the laser cavity as an actuator for the PLL. Prior to the construction of the PLL system, the laser was indirectly stabilized. Plexiglass is being the raw material; a strong encasing of the laser was built to minimize environmental fluctuations in the vicinity the laser. Although the encasing would dampen fluctuations and delay their effect on the laser, long term temperature instabilities like daytime-nighttime periods were also taken into account. $0.1^{o}C$ sensitive temperature control ensures to keep the cavity fiber temperature hence the optical path length in set values.

The laser's phase noise was measured to be lower than the free-running DRO's up to 5 kHz offset frequencies. Demonstrations of decreasing phase noise of the locked laser were conducted via the exercise of artificial boost in its phase noise by external disturbances.

The stabilization of the repetition rate was performed with a 1.3 GHz DRO as the reference oscillator and 32^{th} harmonic of the laser as the test oscillator. The PLL system handles locking ranges of ± 3 kHz around the center frequency of 1.3 GHz. It promises to keep synchronization over short and long time scales. A period of 41.3 hours was recorded as the system stayed in lock where the amount of this period was not dictated by the lifetime of the locking, but the limitations of measurement devices and computers. Disregarding intentional shutting offs, the loop was observed to run for several weeks without any problem.

Finally, the success of repetition-rate might be improved by replacing the free-running DRO with a crystal reference phase-locked DRO which makes a more stable reference. In addition to adding short term stability to the laser with a DRO reference oscillator, long term stability can also be implemented using atomic-transition based references (i.e. Rubidium stabilized diode laser) as reference oscillators in the PLL.

Bibliography

[1] R. H. Stolen, E. P. Ippen, and A.R.Tynes, "Raman Oscillation in Glass Optical Waveguide," Appl. Phys. Lett. **20,** 62 (1972).

[2] E. P. Ippen and R. H. Stolen, "Stimulated Brillouin scattering in optical fibers," Appl. Phys. Lett. **21**, 539-541 (1972).

[3] R. G. Smith, "Optical power handling capacity of low loss optical fibers as determined by stimulated Raman and Brillouin scattering," Appl. Opt. **11**, 2489-2494 (1972).

[4] R .H. Stolen and A. Ashkin, "Optical Kerr effect in glass waveguide," Appl. Phys. Lett. **22**, 294-296 (1973).

[5] R. H. Stolen, J. E. Bjorkholm, and A. Ashkin, "Phase-matched three-wave mixing in silica fiber optical waveguides," Appl. Phys. Lett. **24**, 308-310 (1974).

[6] K. O. Hill, D. C. Johnson, B. S. Kawasaki, and R. I. MacDonald, "CW three-wave mixing in single-mode optical fibers," J. Appl. Phys. **49**, 5098-5106 (1974).

[7] R. H. Stolen, "Phase-matched-stimulated four-photon mixing in silica-fiber waveguides," IEEE J. Quantum Electron. **11**, 100-103 (1975).

[8] A. Hasegawa and F. Tappert, "Transmission of stationary nonlinear optical pulses in dispersive dielectric fibre: Normal dispersion," Appl. Phys. Lett. **23**, 142 (1973); "Anamolous dispersion," Appl. Phys. Lett. **23**, 171 (1973).

[9] L. F. mollenauer, R. H. Stolen, and J. P. Gordon, "Experimental Observation of Picosecond Pulse Narrowing and Solitons in Optical Fibers,*"* Phys. Rev. Lett. **45**, 1095-1098 (1980).

[10] I. N. Duling III, "Subpicosecond all-fibre erbium laser," Electron. Lett. **27**, 544-545 (1991).

[11] K. Tamura, C. R. Doerr, H. A. Haus, and E. P. Ippen, "Soliton fiber ring laser stabilization and tuning with a broad intracavity filter," IEEE Phot. Tech. Lett. **6**, 697-699 (1994).

[12] K. Tamura, E. P. Ippen, H. A. Haus, and L. E. Nelson, "77-fs pulse generation from a stretched-pulse mode-locked all-fiber ring laser," Opt. Lett. **18**, 1080-1082 (1993).

[13] F. Ö. Ilday, J. R. Buckley, W. G. Clark, and F. W. Wise, "Self-similar evolution of parabolic pulses in a laser," Phys. Rev. Lett. **92**, 3902-3905 (2004).

[14] J. R. Buckley, F. Ö. Ilday, F. W. Wise, "Femtosecond fiber lasers with pulse energies above 10 nJ," Opt. Lett. **30**, 1888-1890 (2005).

[15] A Chong, J Buckley, W Renninger, F Wise, "All-normal-dispersion femtosecond fiber laser," Opt. Exp. **14**, 10095-10100 (2006).

[16] F. Ö. Ilday, J. Buckley, L. Kuznetsova, and F. W. Wise, "Generation of 36-femtosecond pulses from a ytterbium fiber laser," Opt. Exp. **11**, 3550-3554 (2003).

[17] R. W. Boyd, *Nonlinear Optics* (Academic Press, 2003).

[18] G. P. Agrawal, *Nonlinear Fiber Optics* (Academic Press, 2007).

[19] G. P. Agrawal, *Applications of Nonlinear Fiber Optics* (Academic Press, 2001).

[20] P. W. Milonni and J. H. Eberly, *Lasers* (Wiley Interscience, 1988).

[21] G.P. Agrawal, "Optical Pulse Propagation in Doped Fiber Amplifiers," Phys.Rev.A **44**, 7493-7501 (1991).

[22] H. A. Haus, E. P. Ippen, and J. G. Fujimoto, "Structures for Additive Pulse Mode Locking," J. Opt. Soc. Am. B **8**, 2068-2078 (1991).

[23] M. Hofer, M. E. Fermann, F. Haberl, M. H. Ober, and A. J. Schmidt, "Mode Locking with Cross-Phase and Self-Phase Modulation," Opt. Lett. **16**, 502-504 (1991).

[24] K. Tamura, E. P. Ippen, H. A. Haus, and L. E. Nelson, "77-ps Pulse Generation from a Stretched-Pulse Mode-Loced All Fiber Ring Laser," Opt. Lett. **18**, 1080-1082 (1993).

[25] K. Tamura, E. P. Ippen, H. A. Haus, "Pulse dynamics in stretched-pulse fiber lasers," App. Phys. Lett. **67**, 158-160 (1995).

[26] A. Chong, J. Buckley, W. Renninger, and F. Wise, "All-normal-dispersion femtosecond fiber laser," Opt. Express **14**, 10095-10100 (2006)

[27] H. A. Haus, J. G. Fujimoto, and E. P. Ippen, "Analytic theory of additive pulse and Kerr lens mode locking," IEEE J. Quantum Electron. **28**, 2086-2096 (1993).

[28] B. Oktem, F. Ö. Ilday, "Spectrally Breathing Self-Similar Femtosecond Pulses from a Highly Nonlinear Er.-Doped Fiber Laser," (to be published).

[29] J. M. Dudley, Ch. Finot, D. J. Richardson, and G. Millot, Nature Phy. **3**, 597 (2007).

[30] A. A. Afanasev, V. I. Kruglov, B. A. Samson, R. Jakyte, and V. M. Volkov, J. Mod. Opt. **38**, 1189 (1991).

[31] C. R. Menyuk, D. Levi, and P. Winternitz, Phys. Rev. Lett. **69**, 3048 (1992).

[32] T. M. Monro, P. D. Millar, L. Poladian, and C. M. de Sterke, Opt. Lett. **23**, 268 (1998).

[33] M. Soljacic, M. Segev, and C. R. Menyuk, Phys. Rev. E **61**, R1048 (2000).

[34] G. I. Barenblatt, *Scaling, Self-similarly and Intermediate Asymptotics* (Cambridge University Press, 1996).

[35] V. I. Kruglov, A. C. Peacock, J. M. Dudley, and J. D. Harvey, Opt. Lett. **25**, 1753 (2000).

[36] M. E. Fermann, V. I. Kruglov, B. C. Thomsen, J. M. Dudley, and J. D. Harvey, Phys. Rev. Lett. **84**, 6010 (2000).

[37] D. Anderson, M. Desaix, M. Karlsson, M. Lisak, and M. L. Quiroga-Teixeiro, J. Opt. Soc. Am. B **10**, 1185 (1993).

[38] K. Tamura and M. Nakazawa, Opt. Lett. **21**, 68 (1996).

[39] F. Ö. Ilday, J. R. Buckley, W. G. Clark, and F. W. Wise, Phys. Rev. Lett. **92**, 213902 (2004).

[40] *Rohde&Schwarz: RF-Spectrum analyzer FSUP26,* http://www2.rohde-scwarz.com

[41] *Dallas Semiconductor: Application Note 3359, Clock (CLK) Jitter and Phase Noise Conversion.* http://pdfserv.maxim-ic.com/en/an/AN3359.pdf.

[42] *Mini-Circuits: Low-noise amplifier ZRL-1150LN+ and Frequency mixer ZX05-5+,* http://www.minicircuits.com.

[43] *Lorch Microwave: Bandpass Filter 4CF2-1300/13-S,* http://www.lorch.com.

[44] *Poseidon Scientific Instruments: Dielectric Resonator Oscillator DRO-1.300-FR*, http://www.psi.com.au.

[45] *Electro-Optics Technology, Inc: Photodiode ET-3500F,* http://www.eotech.com.